frontiers
in Applied Mathematics
and Statistics

TYPE Original Research
PUBLISHED 22 June 2026
DOI 10.3389/fams.2026.1831903



OPEN ACCESS

EDITED BY
Fahad Al Basir,
Asansol Girls' College, India

REVIEWED BY
Selim Reja,
Indian Statistical Institute, India
Abhishek K. Verma,
Forest Research Institute, India
Deepika Sorahia,
Central Agricultural University, India

*CORRESPONDENCE
Sinchan Ghosh
gsinchanpostdoc@gmail.com

RECEIVED 16 March 2026
REVISED 24 April 2026
ACCEPTED 01 May 2026
PUBLISHED 22 June 2026

CITATION
Ghosh S and Singh S (2026) Adaptive stability of the Black alder ecoepidemic system: integrated intervention alone prevents regime shift under phenological variability.
*Front. Appl. Math. Stat.* 12:1831903.
doi: 10.3389/fams.2026.1831903



# Adaptive stability of the Black alder ecoepidemic system: integrated intervention alone prevents regime shift under phenological variability

Sinchan Ghosh[1]* and Shipra Singh[2]

[1]Agriculture Forestry Ecosystem Services Group, Biodiversity and Natural Resources Program, International Institute for Applied Systems Analysis, Laxenburg, Austria, [2]Biodiversity, Ecology, and Conservation Group, Biodiversity and Natural Resources Program, International Institute for Applied Systems Analysis, Laxenburg, Austria

The phylophagous beetle *(Agelastica alni)* larvae outbreak defoliate the canopy in Black alder *(Alnus glutinosa)* dominated forests. Phytochemical defense of plants provides resistance against further beetle outbreaks. A tachinid parasitoid (Meigenia mutabilis) of the beetle, and optimal foraging of generalist passeriforms, provide resilience against the outbreak. Vernal growth enables recovery of the canopy. These resistance, resilience, and recovery processes operate at different time scales and are subjected to climate and management-dependent phenology. Under phenological variability, this eco-epidemic system of plant-pest-parasitoid-predator can adapt its stability or shift its regime from coexistence. In this study, we developed a process-based hybrid seasonal–annual model to examine the adaptive stability against regime shift of this system across nine phenological scenarios. We then applied optimal control theory to compare the cost and benefit of three management strategies against regime shift: parasitoid release, parasitoid release plus larval removal, and a fully integrated strategy including bird-habitat enhancement. Our results showed that, across the phenological variability, the coexistence equilibrium was the least frequently stable regime, whereas the parasitoid-free state was the most frequent. Only the fully integrated management delivered a locally stable managed equilibrium at minimum cost to maintain the coexistence equilibrium.

KEYWORDS
**alluvial forest conservation, ecoepidemic model, ecological resilience, host–parasitoid dynamics, intraguild predation, optimal control theory, phenological mismatch, regime shift**

## 1 Introduction

Black alder (*Alnus glutinosa*) dominates European riparian zones and supports diverse flora and associated fauna habitats [Habitats Directive 92/43/EEC; [1]]. Outbreaks of the phyllophagous leaf beetle (*Agelastica alni*) can substantially defoliate the black alder canopy [2]. Under recurring defoliation from outbreaks, the forest system may collapse due to its vulnerability to other environmental perturbations [3]. An induced physiological change is evident in black alder that offers a stand-level resistance under beetle attack [2]. The black alder canopy recovers via reflushing of leaves after defoliation [2], but repeated

outbreaks can potentially constrain the recovery of the whole canopy due to depletion of carbohydrates beyond a critical level [4–6]. Therefore, a potential full recovery is expected to occur mostly through vernal growth during the next spring following the outbreak season. A resilience of the black alder forest system comes from two natural enemies of beetle larvae that can control the outbreak and aid faster recovery. One is *Meigenia mutabilis*, a koinobiont larval endoparasitoid that parasitises beetle larvae and kills the host larva during emergence [2, 7]. Another control comes from the predation of generalist birds that follows optimal foraging. Optimal foraging theory and empirical studies on a few generalist avian diets suggest that passeriform birds may exploit locally abundant prey, i.e., the leaf beetle, during the outbreaks [8, 9, 85]. To prevent canopy loss from the beetle, management interventions in alder-dominated habitats include biological control of larvae and augmentation of natural enemies [10, 11]. The stand-level resistance, vernal regrowth-dependent recovery, and dual resistance from optimal foraging and parasitoid-mediated resilience form a tractable framework to test the stability of the ecoepidemic system as an adaptive property and how to harness the benefit of this adaptivity to plan management intervention better.

This leaf beetle typically causes outbreaks in spring and early summer. During this period, newly flushed alder foliage provides abundant food for larval feeding and development [12]. In response, alder leaves undergo induced phytochemical and physical changes, including increased phenolic content, reduced starch, and hardened leaf traits that collectively deter further beetle foraging. These defenses determine stand-level resistance and help prevent beetle spread to other susceptible trees [2, 13]. At the same time, the koinobiont larval endoparasitoid tracks beetle larval aggregations and parasitises susceptible larvae by ovipositing on their integument. The subsequent emergence of adult parasitoids results in the death of parasitised larvae [2, 7]. Notably, there is no well-studied larval defense against the parasitoid that has been documented. The existing studies of beetles' chemical defenses are directed to deter specialist birds [14]. Despite these defenses against specialist birds, larvae still remain vulnerable to generalist passeriform birds, which select the most abundant prey as a result of their optimal foraging strategy [15]. Ultimately, the timing and intensities of these intricate interactions are dictated by phenological variations subjected to Climatic and management context.

At least nine ecologically relevant phenologies vary in this system, each having documented links to climate. Spring–summer seasonal length, which changes under a warming climate, determines the vernal growth period of the tree for canopy recovery and vulnerability window for beetle to parasitoid attack for resilience against beetle outbreak [2, 16]. Winter severity influences the overwintering survival of both beetle and parasitoid, which together set the effective outbreak intensity for the following season [7, 12]. Parasitoid development rate increases with warmer climate, raising mortality in parasitised larvae [7]. Concurrently, a warmer winter also lowers the baseline mortality in overwintering larvae. Aggregate predation pressure on the beetle from generalist passeriform birds also varies widely [9]. This predation pressure depends on habitat structure, breeding disturbance, local bird community composition, learned avoidance of beetle chemical defense, and the impact of bird-habitat enhancements. Adaptive foliage and growth patterns can also impact beetle-parasitoid interactions in alder forests under recurring beetle attack [2, 13]. The plant adaptation can lead to a lower carrying capacity for the foraging aggregation of beetles, which is a phenological signal for the parasitoid to locate the beetles. So, a decrease in foraging aggregation can lead to a lower parasitoid attack rate [7]. Thus, variability across phenologies jointly shapes the interactions that adapt the system stability via resilience, resistance, and recovery components.

Understanding how these phenological variabilities shape adaptive stability as a property defined by dynamic resistance, resilience, and recovery can offer strategic planning in habitat restoration and especially pest control by minimizing cost and maximizing benefit in two aspects: timing and effort per intervention measures to design a combined strategy. The optimal control theory can help minimize the cost of intervention strategies using the interdependence of these phenologies, intervention measures, and environmental changes [17]. A first step to apply the strategy in the system is to understand the system's equilibria and their ecological desirability. For instance, since there is no direct empirical evidence on the behavioral or visual distinction of the parasitised beetles from susceptible ones, the consumption of both classes can be assumed to be equal by generalist passeriform birds [18]. Under this assumption, bird predation on parasitised larvae can be interpreted as intraguild predation; foraging on parasitised beetle larvae eliminates future parasitoid recruits as endoparasitoid will be killed with beetle larvae before their emergence [19–21]. In a hypothetical parasitoid-free scenario, the generalist passeriform birds can still provide natural regulation of the beetle only during the outbreak, but without sustained parasitoid, the risk of canopy loss increases. Such a hypothetical parasitoid-free equilibrium, even if locally stable, is ecologically undesirable. Consequently, this research focuses on optimizing intervention strategies that maintain coexistence equilibria and identify parameter conditions that may drive the system to an ecologically undesirable equilibria.

Despite detailed empirical investigation into phenologies in this focal ecoepidemic system, the canopy state regime and adaptive stability remain poorly understood. Measuring resistance is challenging and may only provide a limited understanding of the current stage. For instance, it is empirically difficult to quantify the exact thresholds for plant chemical accumulation, required bird diversity, or parasitoid density needed to control the beetle population without risking extinction. In this study, we measure resistance as a loss from the expected outbreak intensity across seasonal and annual scales. We define resilience as the reciprocal of the rate of recovery in annual carrying capacity. However, following Van Meerbeek et al. [22], we view ecological stability as a multidimensional property rather than a single measure. This perspective helps place our focal system within a broader stability framework that includes resistance, resilience, and the ability of the system to remain within the same domain of attraction after perturbation [23, 24]. Here, we use that framework only as a conceptual guide. The actual stability measures are defined using biologically relevant variables from our hybrid seasonal–annual model: low larval density and low cumulative defoliation indicate

strong resistance during the outbreak season, whereas rapid return of annual carrying capacity and system state toward the reference annual equilibrium indicates resilience across years. In this way, Van Meerbeek et al. [22] provide the general language of stability, while our model provides the system-specific quantities used to evaluate the objectives.

Using these definitions, we formulate three aims to advance the understanding of adaptive stability in this ecoepidemic system. This framework can support management planning under optimal control theory. O1. We identify the most probable stable equilibria of the system across all phenological scenarios. To meet this aim, we develop a process-based model that captures phenologies and intervention strategies through parameters. We represent phenological variability via a parameter space of the model. We then search for all possible stable equilibria in this variable parameter space. Next, we test H1: across phenological variability, the system is likely to converge to a desirable coexistence equilibrium, defined by the presence of a canopy, bird, and parasitoid that can prevent future beetle outbreaks if reintroduced. O2. We quantify the probability of the system shifting to an undesirable equilibrium from its current coexistence equilibrium, unless coexistence is the likeliest equilibrium across phenological variabilities. We test H2: changes in certain phenologies, or parameter values, may serve as early warning signals of a shift to an undesirable equilibrium that still maintains stability. If so, we aim to classify them for each potential undesirable equilibrium. O3. We determine the minimal effort needed for three pest control strategies against the leaf beetle to prevent regime shift. Using optimal control, we aim to minimize the cost of effort per strategy [17, 89]. To guide intervention planning, we test three sets of scenarios, ranging from the least costly to the most costly strategy combinations, against all variable phenologies. We do not explicitly study the spatial variability of the system due to limited comprehensive spatially explicit data for the Adler forests across Europe. However, with the phenological variability, we show how the result and our framework are adaptive for any specific black alder forest as an additional dissemination measure. To extend the framework beyond the analyses presented here, we provide an interactive web interface described that allows users to explore how phenological and management parameters shape adaptive stability under site-specific or scenario-specific conditions.

# 2 Methodology

We employ process-based modeling to characterize the system based on established ecological interactions. To clarify our approach, we evaluate stability across parameters by examining persistence, equilibrium shifts, and control performance. The methodology is organized into the following subsections: model setup (§2.1–2.2), stability analysis (§2.3–2.4), numerical study (§2.5), and a web application for result dissemination (§2.6). The model setup (§2.1–2.2) underpins all three objectives by specifying system dynamics and phenological parameters. For Objective 1, stability analysis (§2.3) identifies annual-map fixed points, while the numerical study (§2.5) assesses their frequency across phenological variation. For Objective 2, stability analysis (§2.3–2.4) delineates bifurcation boundaries and regime-shift conditions, and the numerical study (§2.5) quantifies regime-shift probability and ranks phenological drivers of instability using partial-rank correlation. For Objective 3, stability analysis (§2.3) addresses the optimal control problem, and the numerical study (§2.5) compares management strategies according to a lexicographic feasibility-then-cost criterion. The web application (§2.6) facilitates site-specific exploration of results.

## 2.1 Model formulation

The model comprises two coupled modules that operate at distinct temporal scales. Module 1 is a within-season eco-epidemic ordinary differential equation system that characterizes the tri-trophic dynamics during the spring-summer larval vulnerability window of the leaf beetle. Module 2 is an annual discrete recurrence process that connects successive seasons by updating the beetle recruitment cohort, the parasitoid overwintering population, and the implicit alder foliage carrying capacity according to cumulative defoliation damage. All state variables are expressed per hectare of alluvial forest stand. Because resistance emerges within and across seasons, while resilience depends on annual canopy recovery and carrying-capacity return, only a two-timescale model can identify equilibria, regime shifts, and minimal interventions reliably.

Module 1: We consider four within-season state variables over continuous time $\tau \in [0, T]$, where T is the duration of the larval vulnerability window (baseline T = 55 days, range 45–70 days; univoltine phenology of the leaf beetle). We denote $S(\tau)$ as the density of susceptible (unparasitised) beetle larvae, $I(\tau)$ as the density of parasitised ("infected") beetle larvae, and $F(\tau)$ as the density of adult parasitoid flies. $D(\tau)$: cumulative defoliation damage. Population state variables are expressed per hectare of alluvial forest stand, whereas cumulative defoliation damage is represented as a dimensionless fractional quantity. We describe the within-season dynamics of susceptible beetle larvae by:

$$\frac{dS(\tau)}{d\tau} = -\frac{\beta \times F(\tau) \times S(\tau)}{1 + h \times S(\tau)} - \frac{c_B \times B_t \times S(\tau)}{1 + a_B \times (S(\tau) + I(\tau))} - (\mu_S + u_C(\tau)) \times S(\tau). \quad (1)$$

Here $\frac{dS(\tau)}{d\tau}$ is the rate of change of susceptible beetle larval density over the within-season time $\tau$. The first term, $\frac{-\beta \times F(\tau) \times S(\tau)}{1+h \times S(\tau)}$, represents the parasitoidism and follows a Holling type II functional response. Here, β denotes the parasitoid attack rate, and h denotes the parasitoid handling or saturation parameter; together they capture the fact that parasitoid attack increases with host availability but saturates at high larval density because oviposition is time-limited. The second term, $-\frac{c_B \times B_t \times S(\tau)}{1+a_B \times (S(\tau)+I(\tau))}$, represents predation by generalist passerine birds, also in Holling type II form, where total larval density $(S(\tau) + I(\tau))$ determines the saturation of bird consumption. Here, $c_B$ is the per-unit bird-pressure consumption rate, and $B_t$ is an exogenous index of generalist passerine bird pressure in the focal forest stand rather than an explicit bird population state variable. We use an index because bird abundance and community composition are shaped by ecological processes operating beyond the focal stand and beyond the seasonal timescale of the beetle outbreak,

whereas in this model, we require only their aggregate predation pressure on larvae [9]. The parameter $a_B$ is the bird half-saturation or handling parameter and controls how quickly predation approaches saturation as larval density increases. It therefore reflects a saturating consumption process, not learned avoidance. The final term, $(\mu_S + u_C(\tau)) \times S(\tau)$, represents the removal of susceptible larvae through baseline natural mortality and external intervention. Here, $\mu_S$ is a background/baseline mortality rate of larvae from causes other than parasitoidism and bird predation [83], and $u_C(\tau)$ is the time-dependent removal rate of larvae due to direct intervention during the within-season control process, and during the within-season intervention process.

We describe the within-season dynamics of parasitised ("infected") beetle larvae by

$$\frac{dI(\tau)}{d\tau} = \frac{\beta \times F(\tau) \times S(\tau)}{1 + h \times S(\tau)} - \frac{c_B \times B_t \times I(\tau)}{1 + a_B \times (S(\tau) + I(\tau))} - (\mu_I + \delta + u_C(\tau)) \times I(\tau). \quad (2)$$

Here $\frac{dI(\tau)}{d\tau}$ is the rate of infected beetle larvae, the first term, $\frac{\beta \times F(\tau) \times S(\tau)}{1+h \times S(\tau)}$, represents the conversion of susceptible larvae into the parasitised class through oviposition by parasitoid, and thus forms the eco-epidemic core of the system. The second term, $-\frac{c_B \times B_{t\times} I(\tau)}{1+a_B \times (S(\tau)+I(\tau))}$, represents predation on parasitised larvae by generalist passerine birds in the same Holling type II form used for susceptible larvae, with total larval density (S+I) determining saturation. The final term, $(\mu_I + \delta + u_C(\tau)) \times I(\tau)$represents removal of parasitised larvae through background mortality, parasitoid emergence, and external intervention. Here, $\mu_I$ is the background mortality rate of parasitised larvae, which we assume to be at least slightly higher than $\mu_S$ to reflect the additional physiological burden associated with parasitoid development within the host. The parameter δ denotes mortality due to the emergence of the adult parasitoid from the host and therefore represents the delayed lethal effect of parasitoidism; its value is linked to reported tachinid developmental timing and host emergence intervals [7, 25].

$$\frac{dF(\tau)}{d\tau} = \eta \times \delta \times I(\tau) - \mu_F \times F(\tau) + u_P(\tau), F(T) \equiv F_t \quad (3)$$

$\frac{dF(\tau)}{d\tau}$ is the rate of change in the population density of the parasitoid. Here $\eta \times \delta \times I(\tau)$ represents the recruitment of new adult parasitoids: each parasitised larva that undergoes parasitoid-induced death (at rate δ) yields η new adult flies, where η is mathematically the conversion efficiency. For the solitary endoparasitoid, $\eta \leq 1$ (one parasitoid per host); $\eta < 1$ accounts for parasitoid mortality during development within the host. The second term is the natural mortality of adult parasitoid flies. The third term is the parasitoid augmentation control, where $u_{P(\tau)}$, representing management actions that increase parasitoid density (e.g., intentional release of parasitoids in the forests).

$$\frac{dD(\tau)}{d\tau} = K \times (S(\tau) + I(\tau)), D(0) = 0, D(T) \equiv D_t \quad (4)$$

$\frac{dD(\tau)}{d\tau}$ represents the accumulation of the total defoliation damage $D(\tau)$ as an index $(D(\tau) \in [0, 1))$ inflicted by both susceptible and parasitised larvae over the season. The parameter $\kappa$ converts larval density into a fractional defoliation rate. The per-capita defoliation rate κ is taken as independent of larval density because *A. alni* larvae are sedentary leaf feeders whose individual consumption is energy- and gut-limited rather than encounter-limited, and the empirical stand-scale defoliation–growth relationship reported for broadleaf trees is linear [12, 26], with resource-limitation feedback captured at the annual scale via Equation 8. Ecologically, it represents the foraging rate of larvae on the leaves of Black Adler. The terminal value $D(T) \equiv D_t$ represents the end of season defoliation and is passed to Module 2, which determines the reduction in carrying capacity of the beetle for the following year.

Module 2: We model the temporal map of the annual recurrence that links successive within-season modules in this second module following Wiggins et al. [84]. It updates beetle recruitment, parasitoid carryover, and the implicit alder carrying capacity. The key ecological process captured here is the resilience mechanism: the deciduous *Alnus glutinosa* regenerates its entire canopy each spring from new foliage, restoring the carrying capacity for beetle larvae, but only to the extent permitted by the tree's vigor, which is penalized by cumulative defoliation damage from the previous season. This module consists of 5 main equations and 2 additional equations for optimal control and threshold identification for regime shift during stability analyses.

$$S(0) = \frac{R_B \times A_t}{1 + \frac{A_t}{K_t}}, I(0) = 0, F(0) = F_t \quad (5)$$

$S(0)$, the initial susceptible larval density at the start of each season is determined by the Beverton–Holt recruitment function [27], which limits the recruiting cohort At to the current carrying capacity $K_t$ through density-dependent competition for foliage. The Beverton–Holt form is adopted because *A. alni* behavioral ecology is consistent with compensatory, not overcompensatory, density dependence at stand scale ([2, 12, 28–31]; see Annex 2, Model Adequacy for full ecological justification). This choice also isolates instability arising from the tri-trophic interaction from any instability intrinsic to the recruitment function; the Ricker alternative is retained as the structural-robustness control (Annex 2, Step 10). $R_B$ is the annual beetle reproduction rate calculated from its fecundity. No parasitised larvae exist at season onset because parasitoid activity begins only when adult *M. mutabilis* encounter susceptible host larvae within the season. The initial parasitoid density F(0) equals the overwintering carryover $F_t$ from last year t.

$$A_{t+1} = \sigma_A \times S(T), F_{t+1} = \sigma_F \times F(T) \quad (6)$$

At the end of each within-season window, the surviving susceptible larvae S(T) are mapped to the recruiting cohort for the next year $(A_{t+1})$through an overwinter survival fraction $\sigma_A$. This term mathematically represents a single annual survival parameter that captures all the overwintering survivals: pupation in soil, cold-season mortality, adult emergence, mating, and oviposition. Similarly, $\sigma_F$ represents end-of-season adult parasitoid density to next year's initial density, accounting for tachinid puparia overwinter survival.

$$B_t = B_t^{index}(1 + \xi \times u_B(t)) \quad (7)$$

Here $B_t$ is the effective bird pressure in each year is the product of the baseline bird index $B_t^{index}$ (obtained from PECBMS monitoring data or equivalent woodland bird surveys) [88] and a management multiplier $(1+\xi u_B(t))$. The control variable $u_{B(t)}$ represents annual bird-habitat enhancement actions (e.g., nest-box provisioning, structural habitat improvements, reduced disturbance during the breeding season). The parameter $\xi$ scales the management effort to its effect on local bird density, i.e. the increment or change of bird index as a response to management effort $u_B(t)$.

$$K_{t+1} = K_0 \times \exp(-\varphi \times D_t) \tag{8}$$

$K_{t+1}$ is the carrying capacity of consecutive years that captures the core resilience of the system due to inter-annual feedback from cumulative defoliation. $K_0$ is the undamaged baseline carrying capacity (corresponding to a fully recovered canopy from a healthy *Alnus glutinosa* stand). $\exp(-\phi \times D_t)$ is a penalty that depends upon the accumulated damage $D_t$. The penalty reduces proportionally to next year's foliage quality and quantity, as per the empirical findings of Ferretti et al. [26] and Dolch and Tscharntke [2]: broadleaf tree growth decreases by approximately 0.9% per 1% increase in defoliation, and with the induced chemical resistance and persists through the growing season (~133 days) and reduces subsequent beetle herbivory in the following year.

Finally, to analyse the optimal control of the system, we define an objective functional that minimizes the total ecological and management cost of beetle damage and intervention over a multi-year planning horizon of $N$ years, where each year contains one within-season window of duration $T$.

$$J = \sum_t^N \left[ \int_0^T (\omega_D D(\tau) + \omega_S S(\tau) + \frac{c_P}{2} u_P(\tau)^2 + \frac{c_C}{2} u_C(\tau)^2) d\tau + \frac{c_{B,\text{cost}}}{2} u_B(t)^2 + \omega_T D_t \right], \tag{9}$$

where,

$$0 \le u_P(\tau) \le u_{P,\max}, u_C(\tau) \le u_{C,\max}, 0 \le u_B(t) \le u_{B,\max} \tag{10}$$

Here $\omega_D$, $\omega_S$, and $\omega_T$ are the weights that penalize cumulative damage, current larval density, and terminal damage, respectively. Because $D(\tau)$ accumulates over the season, the running penalty $\omega_D$ assigns greater weight to damage sustained later in the season, reflecting the increasing physiological cost of prolonged defoliation. Ecologically, these are the feedback to the carrying capacities for the beetle larvae through accumulation of canopy loss, accumulation of susceptibility to the infection from parasitoid, and accumulation of end-of-season defoliation that reduces the chances of overwintering of the beetles. $c_P$, $c_C$*and* $c_{B,cost}$ are the unit costs for the three respective processes: Unit cost of parasitoid attack on larvae to other forest economy, Unit cost of targeted removal of larvae, Unit cost of bird-habitat conservation. However, for the model retractability, we consider these costs as a fraction of the forest management budget and, therefore, dimensionless.

We define the parasitoid invasion threshold $R_P$ as the capacity of a small parasitoid introduction to grow across one full annual cycle, following the next-generation approach [32] adapted to the hybrid seasonal–annual structure ([33]; Annex 2, Step 6):

$$R_P \equiv \frac{\partial F_{t+1}}{\partial F_t} \left| x_1^* = \sigma_F \frac{\partial F(T)}{\partial F(0)} \right| S(0) = \hat{S}, I(0) = 0, F(0) = 0. \tag{11}$$

Here $\frac{\partial F(T)}{\partial F(0)}$ is the partial derivative obtained from the variational (sensitivity) equations of within season ODE. When the within-season dynamics are evaluated at constant $S(0) \approx \hat{S}$ and constant bird pressure $B_t$. Equation 6 updates beetle recruitment and parasitoid carryover. Equation 7 updates effective bird pressure. Equation 9 defines the control objective. Equation 10 gives the feasible control bounds. Equation 11 defines the parasitoid invasion threshold. We reduce this rigorous definition reduces to the interpretable approximation: $R_P \approx \frac{\eta \times \delta \times \beta \times \hat{S}}{\left(1+h\times\hat{S}\right)\times \mu_F \times \left(\mu_I + \delta + u_C + \frac{c_B \times B_t}{1+a_B \times \hat{S}}\right)}$. $R_P < 1$ denotes eventual parasitoid extinction and a parasitoid-free equilibrium. $R_P > 1$ means the parasitoid can invade and persist, representing the endemic parasitoidism regime where biological control is effective. $R_P = 1$ marks the transcritical bifurcation boundary. This boundary is searched by varying $\beta$, $\eta$, $\mu_F$, $c_B B_t$, and $u_C$; remaining parameters are listed in Annex 1.

## 2.2 Phenological scenarios and parameter mapping

The nine phenological scenarios described in the Introduction are represented in the model through variation of specific parameters. Table S1 maps each scenario to its climate driver, the affected model parameter(s), the baseline value, and the perturbed range. Each range is justified by published literature or biologically constrained priors (Annex 1). In the numerical analyses, the effect of each scenario is first assessed individually (one-at-a-time variation holding other parameters at baseline) to isolate the contribution of each phenology, and then jointly through full Latin Hypercube Sampling across all parameter ranges to capture interactions among scenarios.

## 2.3 Stability analyses

The long-term stability of this system is determined by the annual recurrence map rather than by the within-season ordinary differential equation (ODE) considered in isolation. The within-season ODE (Equations 1–4) characterizes loss and accumulation processes over a finite interval $\tau \in [0, T]$. Setting $\frac{dS(\tau)}{d\tau} = \frac{dI(\tau)}{d\tau} = \frac{dF(\tau)}{d\tau} = 0$ produces within-season pseudo-equilibria, which do not represent ecologically relevant steady states [86]. Since the system is reset annually through recruitment, overwinter survival, and foliage recovery equations [5–8]. Multi-year dynamics, including outbreak recurrence, parasitoid persistence, and tipping risk, are governed by the annual map. The stability analysis is analytically well-posed for our model but does not admit a closed-form solution. Specifically, the annual map G and its structure, existence conditions for fixed points, the Jacobian $J_G$ of the annual map (derived via the chain rule and variational equations), the parasitoid

invasion threshold $R_P$ as the dominant eigenvalue of $J_G$, local stability criteria (spectral radius less than one), and bifurcation conditions (eigenvalue crossing the unit circle) are all derived analytically [92]. In contrast, the seasonal flow $\Phi_T$ and its derivatives are evaluated numerically, as the Holling Type II functional responses render the within-season ODE non-linear and analytically intractable. This approach, which combines analytic stability conditions with numerical evaluation of the seasonal flow, is standard and mathematically rigorous for hybrid eco-epidemic models [33, 34]. The analysis proceeds through a 10-step framework, as detailed in Annex and has been generated via Mathematica, and manual calculation.

The stability analysis addresses the three study objectives through a stepwise analytical structure. For Objective 1 (O1), all ecologically distinct fixed points of the annual map are identified (Step 3). Their local stability is classified using the Jacobian eigenvalues (Step 4). The parasitoid invasion threshold $R_P$ is then computed (Step 6). The analysis scans the full parameter space to determine the frequency of each equilibrium type across phenological scenarios. The equilibrium with the highest frequency is designated as the most probable equilibrium. Objective 2 (O2) is addressed by tracking eigenvalue magnitudes [87] and bifurcation boundaries across parameter space (Step 7). The regime shift probability is computed as the fraction of sampled parameter sets converging to an alternative equilibrium. Parameters are ranked by their influence on bifurcation proximity using the PRCC of the dominant eigenvalue magnitude (Step 10). Parameters identified as drivers of instability become candidate early warning signals if the corresponding phenology is empirically observable and its variation matches the destabilizing parameter direction. Objective 3 (O3) is addressed by optimal control analysis (Step 8) and a three-scenario comparison (Step 9). This compares resistance, resilience, stability, and cost outcomes across parasitoid-only, combined parasitoid-and-bird, and full integrated control, applying a lexicographic decision rule: feasibility first, then minimum cost.

## 2.4 Definitions of resistance, resilience, and tipping during stability analyses

In this study, the framework of Van Meerbeek et al. [22] is used to structure the interpretation of stability, not to replace the model-specific metrics required by the present eco-epidemic system. Their synthesis treats ecological stability as a set of complementary properties that describe how a system responds to perturbation relative to a reference condition and its domain of attraction. We therefore map those general properties onto the quantities generated by our annual map. Resistance is represented by suppression of outbreak intensity, measured through equilibrium defoliation and peak larval load; resilience is represented by the rate of return to the annual equilibrium, measured through the dominant eigenvalue magnitude and return time; and tipping is evaluated from loss of local stability and from ecologically relevant functional thresholds. The parasitoid invasion threshold $R_P$is included as a complementary regime-structure metric for Objective 2, rather than as a direct Van Meerbeek stability component.

We operationalise the first two components for the hybrid seasonal-annual model as follows. All metrics are standardized against a reference state and bounded between $-1$ and 1, enabling comparison across phenological scenarios. We apply these standardized metrics to model-simulated trajectories from the annual recurrence map, treating the map output as the system time series from which the reference value and perturbation response are extracted. Reference state. For each system variable, the reference state $S_R$ is defined as its value at the annual fixed point $x^* = (A^*, F^*, K^*)$. Specifically, resistance is assessed using cumulative defoliation D as the system variable, with $S_R = D^*$ (equilibrium defoliation defined by mean of simulated recurrent defoliation over the year); resilience is assessed using carrying capacity K as the system variable, with $S_R = K^*$ (equilibrium carrying capacity). Different system variables may have different reference states, consistent with the multidimensional treatment of stability [23, 24]. Resistance is the capacity of the system to withstand change during a perturbation [22]. It is measured by the standardized index: $Resistance = 1 - \frac{2|S_R - S_X|}{S_R + |S_R - S_X|}$ (R1), where $S_X$ is the value of the system variable at maximum deviation following a standardized pulse perturbation to the annual map (displacement of $A_t$ by $\pm$ δ% of $A^*$, with δ = 20% as the baseline perturbation magnitude). A resistance value of 1 indicates no deviation from the reference; 0 indicates deviation equal to the reference value. As complementary indicators, we also report the equilibrium cumulative defoliation D* and the peak within-season total larval density $max_\tau [S(\tau) + I(\tau)]$ along the seasonal trajectory starting from fixed-point initial conditions. Resilience is the rate at which the system returns to its reference state after a perturbation [22, 35]. It is measured by the standardized index: $Resilience = \frac{2|S_R - S_0|}{|S_R - S_0| + |S_R - S_Y|} - 1$ (R2), where $S_0$ is the value of the system variable at maximum deviation from the reference (i.e., $S_0 = S_X$ from the resistance measurement), and $S_Y$ is the value after Y annual iterations following the perturbation. We set Y = 5 annual cycles as the standardized recovery window, corresponding to a management-relevant planning horizon. A resilience value of 1 indicates full recovery within Y iterations; 0 indicates no net recovery. As complementary indicators, we report the dominant eigenvalue magnitude $\rho^* = max_i \ |\lambda_i (J_G (x^*))|$ of the annual-map Jacobian at the fixed point and the characteristic return time $T_{return} = -\frac{1}{\ln(\rho^*)}$, which captures asymptotic (linearised) resilience. Eigenvalue-based and trajectory-based resilience provide complementary information: the former reflects the local linear return rate, while the latter captures non-linear dynamics far from the fixed point [36, 37]. The eigenvalue-based and trajectory-based metric sets differ in their mathematical domain of validity; the two need not rank scenarios identically (Annex 2, Step 4).

In the stability analyses, we employ related the basin stability concept of Menck et al. [38], and definition of stability sensu Vanmeerbeek [22]. We define adaptive stability as the capacity of the system to maintain ecological function through the joint action of within-season resistance and annual resilience, where the balance between resistance and resilience adapts to phenological conditions. Unlike engineering resilience (a single return-rate measure; [35]), ecological resilience (a basin-of-attraction measure; [39]), or adaptive capacity (a social-ecological management concept; [40, 91]), adaptive stability captures the multi-timescale interplay in which within-season resistance to outbreak damage and annual recovery of canopy condition jointly determine whether the system persists in a functional regime. Here, "adaptive stability" is used as a descriptive term representing the joint behavior of

resistance (R1) and resilience (R2), rather than a formally distinct theoretical construct. The model contains two mathematically distinct bifurcation structures (§2.3; Annex 2, Steps 1–5): the within-season ODE operates in continuous time with stability boundaries on the imaginary axis, while the annual map operates in discrete time with stability boundaries on the unit circle [33]. Because within-season pseudo-equilibria are not ecologically interpretable as steady states (§2.3), all tipping in this study is defined on the discrete-time annual map. We distinguish three levels of stability loss that may or may not coincide [22, 41].

*(i) Loss of local asymptotic stability:* the dominant eigenvalue magnitude $\rho* = max_i\ |\lambda_i(J_G(x*))|$ crosses the unit circle ($\rho^* \rightarrow 1$), and x* loses its attracting property. The crossing direction determines the bifurcation types: fold, flip, or Neimark–Sacker (33; Annex 2, Step 7).

*(ii) Functional threshold crossing:* The system variable enters a functionally unacceptable range independent of any mathematical bifurcation: the long-run mean defoliation exceeds $D_{crit} = 0.5$ (corresponding to 50% seasonal defoliation; 26), or the carrying capacity $K_t$ falls below $K_{\min} = 0.5$ K0 for three or more consecutive years, indicating persistent canopy degradation. The system may satisfy this criterion while still retaining $\rho^* < 1$, because functional thresholds depend on the magnitude of the state, not on the topology of the attractor.

*(iii) Regime shift:* the annual-map trajectory converges to a structurally different attractor — the parasitoid-free fixed point x1*, the canopy-only state x0*, or a periodic cycle. This can result from the basin of $x_2^*$ vanishing under (i), or from a finite perturbation crossing the basin boundary independently of (i) (Annex 2, Step 7).

The dynamical tipping boundary is the critical parameter value $p_c$ at which $\rho*(p_c) = max_i\ |\lambda_i(p_c)| = 1$ in the annual map (Equation 19). The functional tipping criterion (ii) is evaluated relative to this boundary to determine whether ecological collapse precedes or follows mathematical destabilization.

Regime shift probability and parametric drivers of instability for O2. The probability of regime shift is defined as the fraction of N LHS-sampled parameter sets (Step 10) for which the annual map converges to an equilibrium qualitatively different from the coexistence fixed point $x_2^*$. Formally, $P_{shift} = \frac{n_{alt}}{N}$, where $n_{alt}$ is the number of sampled parameter sets yielding a parasitoid-free or trivial equilibrium. This probability is conditional on the assumed uniform distributions over the parameter ranges in Annex 1 and is reported with 95% bootstrap confidence intervals. Parametric drivers of instability are identified by computing PRCC between each model parameter and the dominant eigenvalue magnitude $\rho^*$ across the LHS sample. Parameters with $|PRCC| > 0.25$ that drive $\rho^*$ toward unity are classified as parametric drivers of instability. These parametric drivers can be translated to candidate early warning signals when the phenological process providing ecological meaning to the parameter is empirically observable, and its direction of variation under climatic change matches the destabilizing direction identified by the model. For example, if the model identifies overwinter beetle survival $\sigma_A$ as a parametric driver whose increase destabilizes coexistence, and if milder winters observably increase $\sigma_A$ Then, declining winter severity constitutes a candidate early warning signal for regime shift. As a focused analysis within O2, we compute $R_P$ across the full range of the bird pressure index $B_t \in [0.5, 2.0]$ at the calibrated baseline, and across the $(\beta, B_t)$ parameter plane, to map the transcritical bifurcation boundary separating the coexistence and parasitoid-free regimes.

## 2.5 Numerical analyses

The numerical analyses are conducted across all nine phenological scenarios (Table S1), first by one-at-a-time parameter variation to isolate the effect of each scenario, and then by joint Latin Hypercube Sampling (JLHS) across all parameter ranges to capture interactions. The absence of long-term, site-specific time series for Beetle outbreak density, M. mutabilis parasitoidism prevalence, and passerine kill rates on this beetle challenges only numerical simulation-based analyses. Therefore, we focus on the system characteristic through mapping the structural stability landscape of the system and calibration for parameter ranges per regime. This technique allows us to identify parameter combinations and control allocations that support a stable low-damage equilibria: those that induce tipping, and the response of the parasitoid invasion threshold $R_P$ to intraguild predation and control effort. However, this analysis therefore restricts us from aiming to predict site-specific outbreak timing or magnitude without site-specific time series data. Stability properties, including fixed-point existence, eigenvalue conditions, and bifurcation type, are determined by the structure of the annual map and the qualitative nature of the functional responses in our simulation for a range of plausible values based on stability analyses in Annex 2 and known parameter values in Annex 1. We follow this parameter range for simulation in the standardized protocol in theoretical eco-epidemic modeling, as it is in Chattopadhyay and Arino [42] and Hethcote et al. [43].

During numerical analyses, parameters were divided into four classes: biological baseline parameters, calibrated structural parameters, bounded management controls, and objective-function weights. Biological parameters were assigned from empirical studies, cross-system proxies, or biologically constrained priors as summarized in Annex 1. Structural parameters lacking direct estimates but required for scale consistency or threshold behavior, including $\beta$, $c_B$, and $\kappa$, were calibrated so that the model reproduced plausible baseline parasitoidism, daily bird predation, and proportional defoliation. The management variables $u_P(\tau)$, $u_C(\tau)$, and $u_B(t)$were not treated as ecological constants, but as bounded decision variables with baseline value zero. The weights in the objective functional were treated as scenario-dependent management preferences rather than empirically fixed ecological parameters.

To address the lack of precise parameter estimates, the analysis employs two complementary safeguards. First, all uncertain parameters are represented as intervals, as specified in the parameter tables of Annex 1, with empirically justified ranges. Stability and control outcomes are reported as robust regions within parameter space rather than as point estimates; conclusions are accepted only if valid across each parameter's entire range. Second, structural robustness is assessed by replacing baseline functional forms with ecologically plausible alternatives: Beverton–Holt vs. Ricker recruitment in Equation 5, Holling Type II vs. linear bird predation, and S → I compartmental parasitoidism vs. direct

parasitoid-induced mortality. All three qualitative conclusions (O1–O3) are preserved under both parametric and structural perturbations, confirming them as properties of the tri-trophic interaction architecture rather than artifacts of specific modeling assumptions (Annex 2, Table 2).

For each equilibrium and each control scenario, we compute the resistance metrics $D^*$ and $\max_\tau [S(\tau) + I(\tau)]$, the resilience metrics $\rho^*$ and $T_{return} = -\frac{1}{\ln(\rho^*)}$, and cumulative control cost $J$ where relevant. A perturbation-recovery time obtained by iterating the annual map from a standardized displacement of the fixed point, so that the relative performance of parasitoid-only and combined control strategies can be compared on resistance, resilience, and cost grounds.

## 2.6 Interactive exploration of the modeling framework

To make the framework directly explorable, we developed AlderIPM-Sim Web, a browser-based interface that reimplements the seasonal–annual model of §2.1 and the analyses of §2.3–2.5 in JavaScript (https://gsinchanpostdoc.github.io/AlderIPM-Sim/). We used JavaScript implementation mirroring the Python pipeline used to generate all results in this manuscript, with the calibrated parameter set in Annex 1 as the default state, so that the default app output reproduces the baseline results reported in this article. Users can adjust the nine phenological parameters flagged in Table S1, the three management controls), and the objective-function weights. Structural parameters and functional-form choices are not user-adjustable because they define the model class under which the stability conclusions of our result holds. Altering them would produce a different model, not a parameterisation of this one. All analyses are computed live in the browser: single-parameter scans, the parasitoid invasion threshold, resistance and resilience metrics, and optimal-control trajectories under the receding-horizon forward–backward sweep method. The joint Latin Hypercube sensitivity analysis (Figure 1A) is not exposed in the live interface because the sample sizes required for stable PRCC estimates are computationally prohibitive in a browser; the pre-computed results from our parameter sets and results are shown instead. Consistent with tthe model and methods described in this article, the tool is intended for exploration of structural behavior under phenological and management variability, not for site-specific prediction, which would require empirical time-series data on beetle outbreak density, parasitoidism prevalence, and passerine predation from the target habitat. The app source code and the underlying simulation pipeline are released under the MIT license at the repository linked above and in the Data Availability Statement.

# 3 Results

The results of this study are grouped by each objective. Each subsection from 3.1 to 3.3 reports the metrics that directly test the corresponding hypothesis.

## 3.1 Meeting objective 1

Figure 2 shows 3 outputs from stability analyses: Annual equilibria identified as fixed points of the yearly recurrence map (Step 3), their local stability classified from the Jacobian eigenvalues of that annual map (Step 4), and the frequency of each equilibrium occurs across Latin Hypercube Sampling under parameter space (Step 10). Figure 2A reports the stable-presence probability, i.e., the fraction of sampled parameter sets for which a given equilibrium exists as a locally stable fixed point of the annual map. In this sense, the parasitoid-free equilibrium canopy-only is the most frequent stable regime across parameter space, whereas the coexistence equilibrium parasitoid-free is the least frequent stable regime found across the parameter space. The stable presence probability of the parasitoid-free equilibria is closest to the coexistence equilibria. Therefore, under continuous variable phenology, the phenological mismatch can lead to a parasitoid-free equilibrium where the beetle outbreak is regulated by birds, and eventually the system is likely to jump into a stable equilibrium where the beetle is also absent. This result indicates rejection of the H1: under all variability in phenologies, the system is likely to converge to a desirable coexistence equilibrium, defined by the presence of a canopy, bird, and parasitoid that can prevent future beetle outbreaks if reintroduced.

Following the rejection of H1, Figure 3 presents the predicted stable fixed point of the annual map and the equilibrium damage $D^*$ at the coexistence equilibrium. The results are displayed as a function of individual parameter variability, excluding parasitoid invasion risk as a stability driver. This analysis demonstrates the persistence of coexistence across different phenology variability ranges. Although most phenologies and associated parameters covary in natural systems, examining individual variation reveals the system's maximum potential. Among nine one-at-a-time parameter scans, seven parameters altered the equilibrium class. Bird pressure ($B_t$) and the foliage-memory penalty ($\varphi$) did not induce regime shifts within the scanned range. Season length (T) influenced defoliation damage but did not transition the system to alternative equilibria within the examined range. Nevertheless, because defoliation damage responds rapidly to changes in T, a regime shift may occur over a longer temporal scale. Notably, reducing the parasitoid attack rate $\beta$, parasitoid overwinter survival $\sigma_F$, or the parasitoid emergence rate $\delta$ each caused a transition from coexistence to herbivore dominance, whereas increasing the beetle reproduction ratio $R_B$ facilitated parasitoid invasion, directly affecting system stability and the resulting equilibrium class.

The most pronounced regime shift is driven by the parasitoid attack rate β. As β increases, system outcomes transition from the absence of parasitoids to coexistence, accompanied by a rapid reduction in equilibrium damage. The beetle reproduction ratio $R_B$ delineates three distinct regimes: at low, beetles are unable to persist, and only trees remain; at intermediate, beetles persist without parasitoids and inflict canopy damage; at high, host density supports parasitoid establishment, resulting in stable coexistence. Increasing susceptible larval mortality $\mu_S$ initially disrupts parasitoid persistence by limiting host availability, and at higher values, beetles are eliminated, restoring the system to

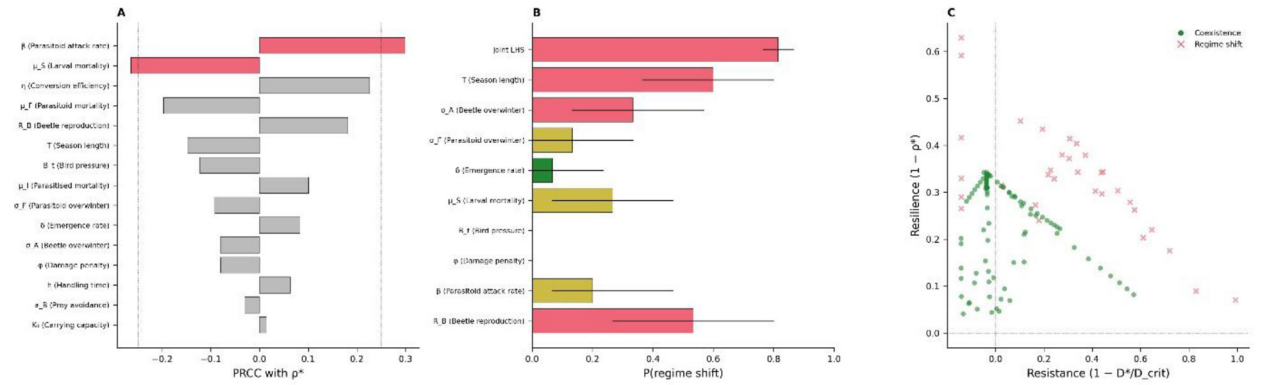


FIGURE 1
Early-warning summary: parametric drivers, regime-shift probability, and adaptive-stability reference frame. **(A)** Partial rank correlation coefficients (PRCC) between each model parameter and the dominant eigenvalue magnitude $\rho^*$ across the Latin Hypercube sample; red bars indicate |PRCC| > 0.25 (warning candidates). **(B)** Regime-shift probability per phenological scenario (one-at-a-time variation) and for the joint Latin Hypercube sample; horizontal bars show 95% bootstrap confidence intervals; color indicates risk level. **(C)** All one-at-a-time scan points projected onto the resistance–resilience plane, where resistance $= 1 - \frac{D}{D_{crit}}$ and resilience $= 1 - \rho^*$ (contrast to van Meerbeek et al. [22] resistance and resilience); green circles denote coexistence outcomes, red crosses denote regime shifts.

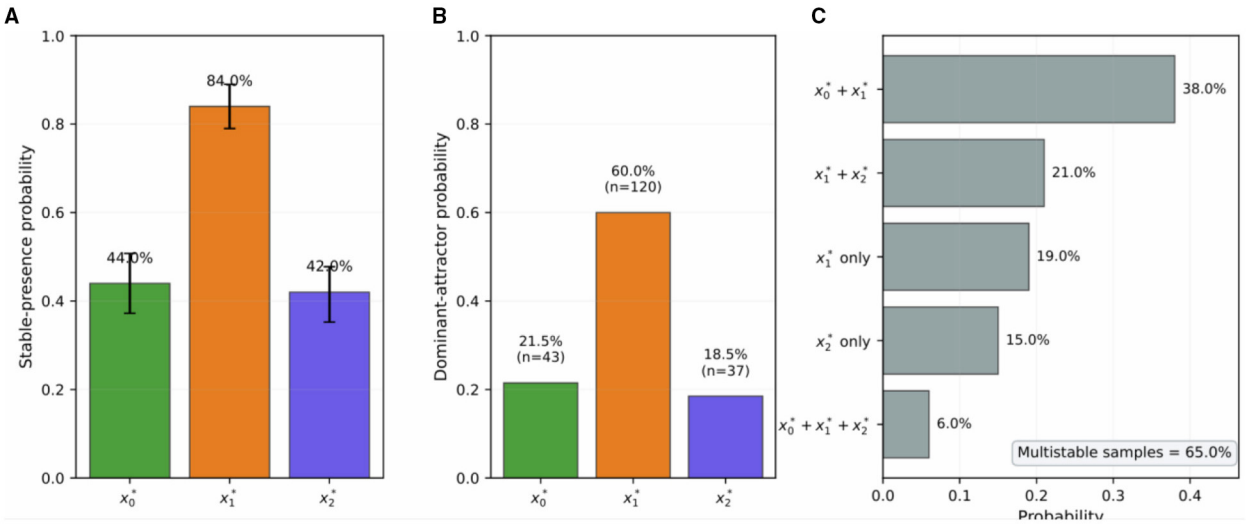


FIGURE 2
Equilibrium landscape across the phenological parameter space. $x_0^*$, $x_1^*$, $x_2^*$ are canopy-only, parasitoid-free, and coexistence equilibria. No degraded equilibria (i.e., carrying capacity below half the threshold value) were found. **(A)** Baseline fixed points of the annual map at calibrated parameters; bar length indicates equilibrium beetle density A*, with spectral radius $\rho^*$ and stability status annotated. **(B)** Fraction of the Latin Hypercube–sampled parameter space in which each equilibrium class exists as a locally stable fixed point; bars can exceed unity in sum due to multistability. **(C)** Dominant-attractor frequency: the fraction of sampled parameter sets for which the annual map trajectory converges to each class from the coexistence reference initial condition; multistability rate annotated.

an intact canopy. Thresholds for regime shifts are also observed in beetle overwinter survival $\sigma_A$ and parasitoid survival, with coexistence possible only above critical values. For the parasitoid emergence rate δ, coexistence is maintained only above a specific threshold; otherwise, the system remains parasitoid-free. Increasing bird pressure Bt does not create regime boundaries but alters equilibrium beetle and damage levels. Birds suppress beetle populations, reducing damage, and remove parasitised larvae, thereby weakening parasitoids. Consequently, their net effect modifies quantitative but not qualitative equilibrium classes within the scanned range. The phase plane illustrates how attack rate and bird predation influence equilibria (Figure 4). Higher bird predation increases the attack rate required for coexistence, which predominantly occurs at high attack rates and low-to-moderate predation (71% of the grid). The parasitoid-free regime is observed at low attack rates or high predation (27% of the grid). Coexistence is achieved when parasitoid attack rate, winter survival, emergence rate, beetle reproduction and survival are high, larval mortality is low, and passerine predation is moderate, assuming other phenologies are held constant.

Figure 5 evaluates the parasitoid invasion threshold, $R_P$, at the parasitoid-free fixed point of the annual map, in contrast to the durability of the coexistence equilibrium. $R_P$ measures the annual growth potential of a rare parasitoid at the boundary equilibrium.

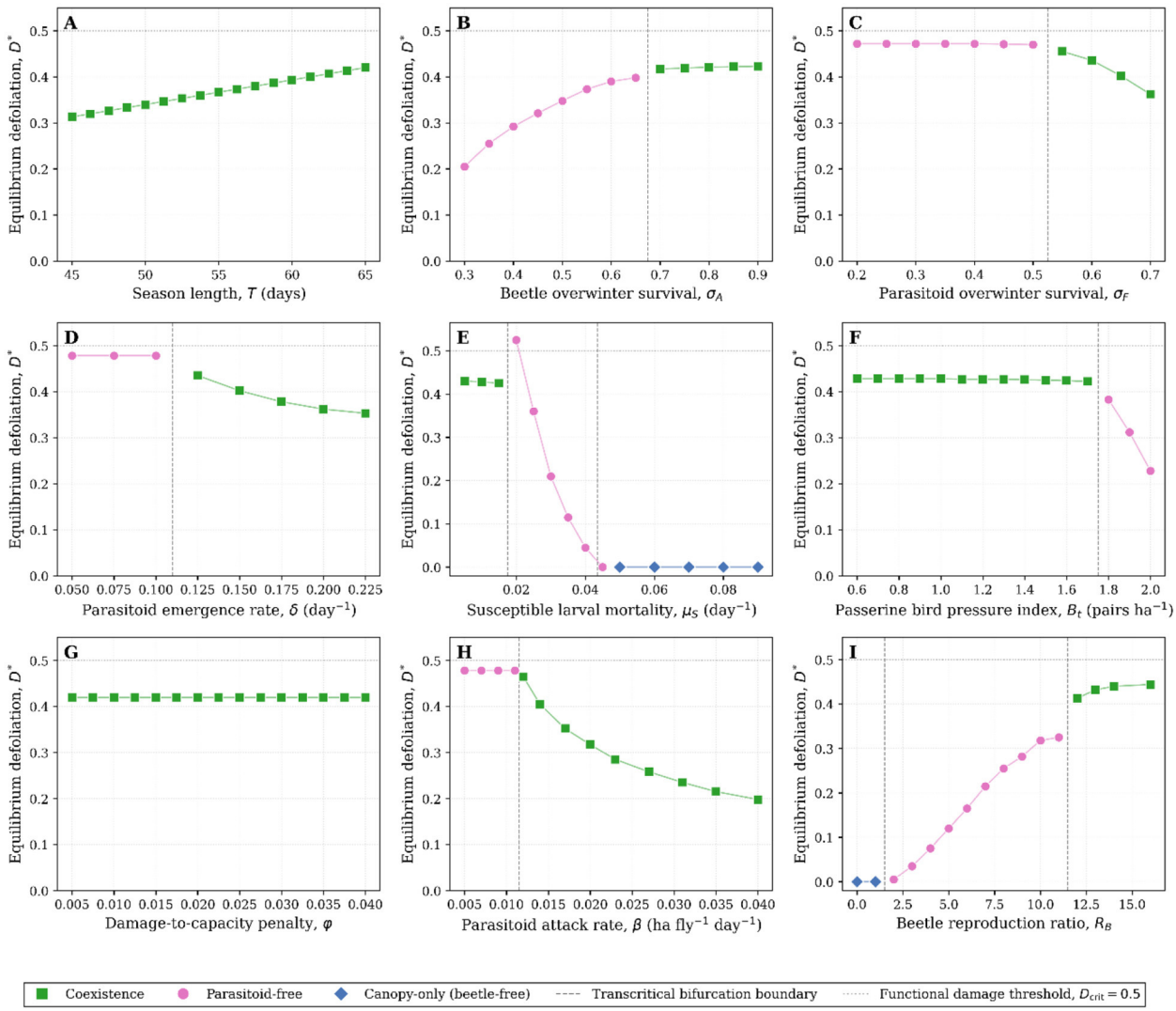


FIGURE 3
Equilibrium transition boundaries across all nine phenological scenarios and the pairwise $\beta \times B_t$ parameter plane. **(A-I)** show equilibrium damage D* at the stable fixed point of the annual map as each phenological parameter is varied individually across its plausible range (one-at-a-time scans; all other parameters held at the calibrated baseline). Green squares: coexistence equilibria; pink circles: parasitoid-free equilibria; blue diamonds: canopy-only (beetle-free) equilibria; teal triangles: coexistence non-fixed-point attractors. Connecting lines trace the equilibrium branch within each class. The horizontal dotted line marks the functional damage threshold $D_{crit} = 0.5$. **(A)** Season duration T. **(B)** Beetle overwinter survival $\sigma_A$. **(C)** Parasitoid overwinter survival $\sigma_F$. **(D)** Parasitoid emergence rate δ. **(E)** Susceptible larval mortality $\mu_S$. **(F)** Passerine bird pressure index $B_t$. **(G)** Damage-to-capacity penalty $\varphi$. **(H)** Parasitoid attack rate β. **(I)** Beetle annual reproduction ratio $R_B$.

If $R_P$ exceeds 1, parasitoids can increase from rarity and drive the system toward coexistence; if $R_P$ is less than 1, they fail to establish, and the parasitoid-free state persists. The line $R_P = 1$ marks the invasion boundary between these regimes. This threshold measures how many new adult parasitoids are produced for each added per year, calculated at the parasitoid-free equilibrium of the annual map across other parameter space (Step 6). Since H1 is rejected, the parasitoid-free state is likely. Thus, $R_P$ is crucial for O2. If $R_P > 1$, a few parasitoids can spread and push the system to coexistence. If $R_P < 1$, they die out, and the system remains parasitoid-free. The $R_P = 1$ line marks where the main shift between these two states occurs. Seven of nine parameters cross the $R_P = 1$ threshold. Raising the bird pressure index $B_t$ quickly lowers $R_P$ and crosses the threshold. Increasing the susceptible larval death rate $\mu_S$ also lowers $R_P$ and crosses the threshold. Conversely, increasing the parasitoid attack rate β raises $R_P$ and crosses the threshold. Higher $R_B$ increases $R_P$ with persistence around the threshold value of $R_B$ from Figure 3. Beetle overwinter survival $\sigma_A$ (Figure 5B), parasitoid overwinter survival $\sigma_F$ (Figure 5C) and increasing parasitoid emergence rate δ (Figure 5D) each raises $R_P$. Each threshold crossing shows the parameter value needed for persistence. Season duration T (Figure 5) increases $R_P$, so longer seasons lower but do not eliminate parasitoid persistence at baseline. The defoliation damages memory-based vernal growth $\varphi$ (Figure 5G), which defines carrying capacity, slightly decreases $R_P$. This shows that foliage-memory feedback has minimal impact on parasitoid invasion. Therefore, Figure 5 reveals that moving from coexisting equilibria by decreasing $R_P$ results from a lower attack rate, reduced beetle or parasitoid survival, or slower emergence.

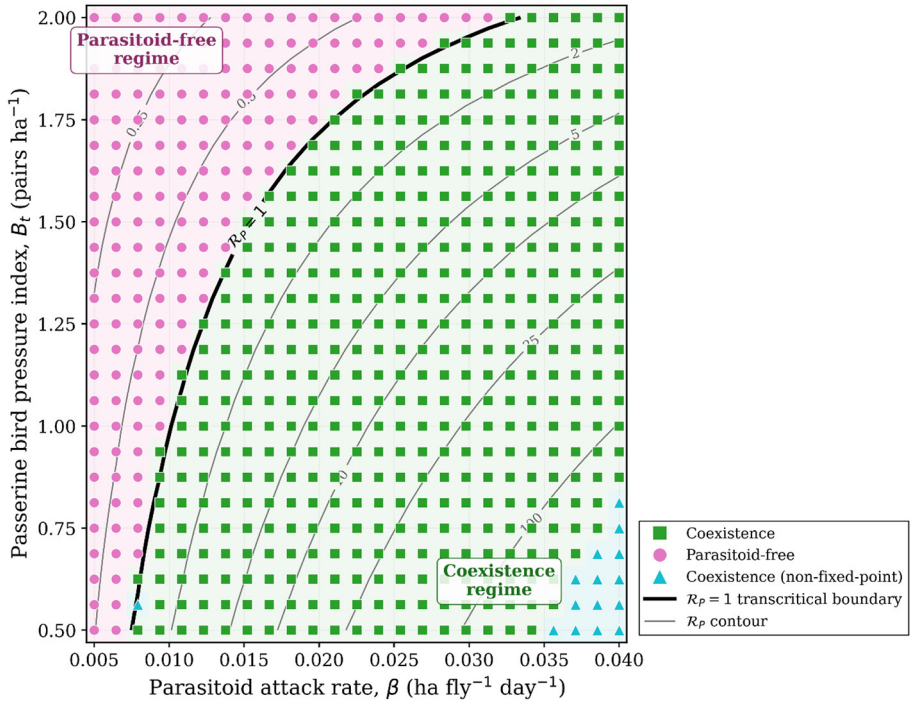


FIGURE 4
Pairwise phase plane in the β × $B_t$ parameter space. Gray contours indicate values of the parasitoid invasion threshold $R_P$; the bold black curve marks $R_P = 1$, the transcritical bifurcation boundary separating the coexistence regime (lower-right) from the parasitoid-free regime (upper-left). Green squares: coexistence equilibria; pink circles: parasitoid-free equilibria; teal triangles: coexistence non-fixed-point attractors. The diagonal orientation of the boundary reflects the intraguild predation mechanism; increasing bird pressure progressively raises the parasitoid attack rate required for parasitoid invasion.

## 3.2 Meeting objective 2

Figure 1 quantifies regime-shift risk and highlights the main drivers of parametric instability—variability in phenology (the timing of seasonal biological events). The partial rank correlation coefficient (PRCC) shows how sensitive system stability at coexistence is to each parameter. Stability is measured using the dominant eigenvalue magnitude ρ* (indicating how quickly the system returns to equilibrium after disturbance), based on the Latin Hypercube sample (Step 10) in Figure 1A. Parameters with absolute PRCC above the threshold increase instability risk in ρ*. Only parasitoid attack rate β (the rate at which parasitoids attack hosts) and susceptible larval mortality $\mu_S$ (the death rate of larvae vulnerable to attack) surpass this threshold, but their effects differ; increasing β stabilizes coexistence (positive PRCC, higher ρ*), while increasing $\mu_S$ lowers stability. Next most influential are parasitoid conversion efficiency $\eta$ (the efficiency with which parasitoids develop within hosts) and adult parasitoid mortality $\mu_F$ (the death rate of adult parasitoids), indicating demographic sensitivity. Other parameters, which shift $R_P$ in Figure 5, show moderate PRCC. $R_P$ indicates potential for parasitoid invasion (whether a small number of parasitoids can successfully establish), while ρ* measures the speed of return to coexistence after disturbance.

Figure 1B displays the regime-shift probability for each phenological scenario as well as for joint Latin Hypercube sampling. When all parameters are varied simultaneously, 81.5% of parameter sets force the coexistence equilibrium to shift. Season duration and beetle reproduction $R_B$ are the most likely parameters to induce a regime shift when all parameters vary. Note that season duration variation alone did not show the shift in objective 4. However, in reality, season duration is linked to most phenologies; the Figure 1B observation is most likely in the real world. Beetle overwinter survival $\sigma_A$ and susceptible larval mortality $\mu_S$ also contribute significantly. In contrast, bird pressure $B_t$ and foliage-memory $\varphi$ do not induce regime shifts across sampling, similar to Figure 5, where, upon varying alone, $B_t$ does not cross the $R_P = 1$ threshold from coexistence, and $\varphi$ has minimal impact on $R_P$. The high joint shift probability, here all parameters vary jointly, the regime shift probability is relatively much higher than individual parameter values, which is an obvious assumption, but provides a comparison to individual parameter sensitivity.

Figure 1C projects all single-parameter scan points onto the resistance–resilience plane. Here, resistance is $1 - \frac{D}{D_{crit}}$ and resilience is $1 - \rho*$, which contrasts the resistance and resilience sensu van Meerbeek et al. [22] tested in later Figure 1. Points representing coexistence equilibrium cluster within a region of positive resistance and moderate resilience. Points for parasitoid-free or canopy-only regimes are more scattered and often show higher resilience. This occurs because the parasitoid-free equilibrium can have a smaller ρ* (faster return rate) than coexistence. Thus, resilient systems can remain in undesirable parasitoid-free regimes. This reflects the adaptive behavior of this system's stability.

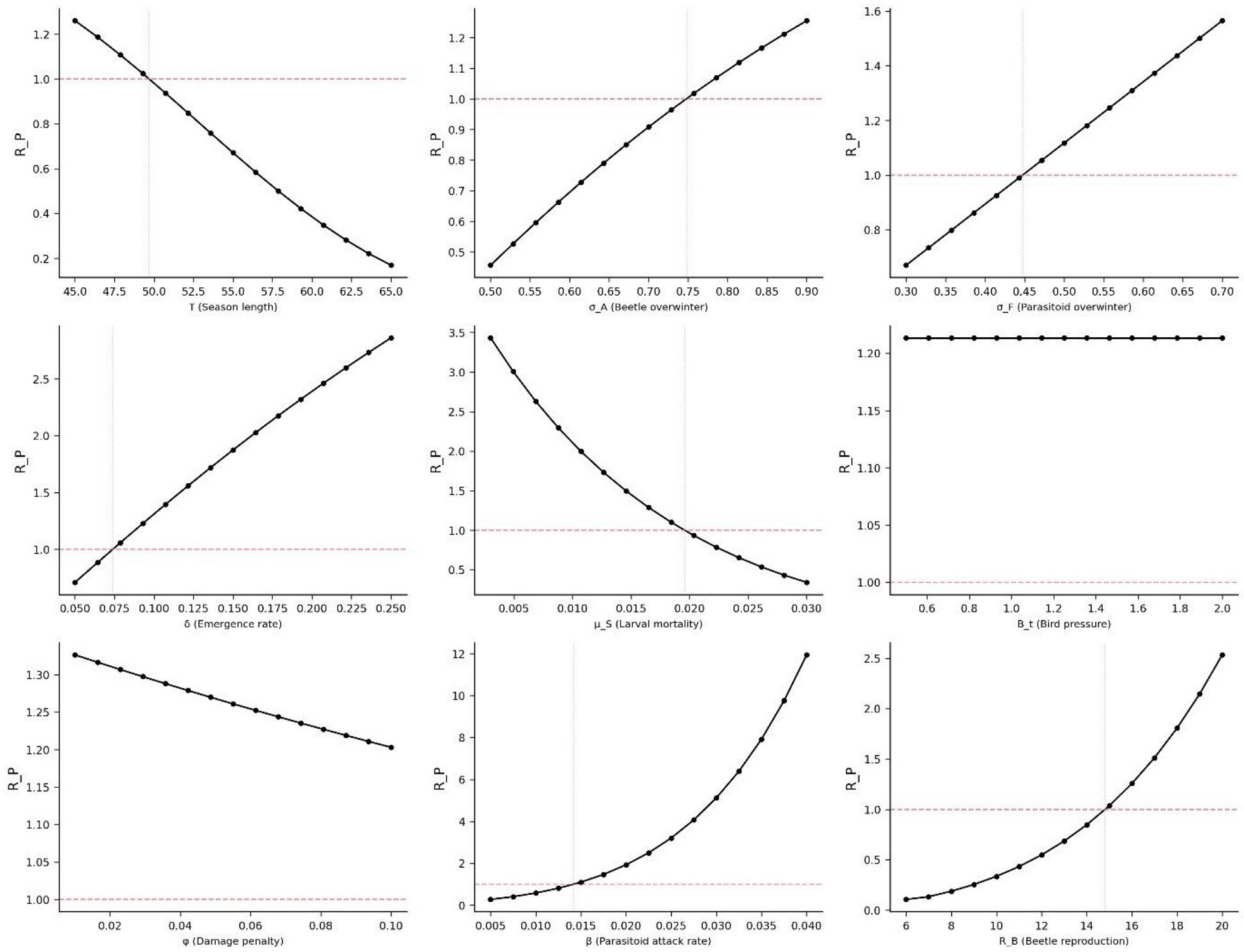


FIGURE 5
Parasitoid invasion threshold $R_P$ as a function of each phenological parameter. Each panel shows $R_P$ evaluated at the parasitoid-free fixed point of the annual map while varying one parameter across its plausible range (Table S1), with all other parameters held at the calibrated baseline. The dashed red line marks $R_P = 1$. Above this boundary, the parasitoid can invade and persist (coexistence regime); below it, the parasitoid declines to extinction (parasitoid-free regime). Vertical dotted lines indicate the approximate parameter value at which the threshold crossing occurs.

Together, these plots support hypothesis H2 that changes in certain phenologies, or parameter values, may serve as early warning signals of a shift to an undesirable equilibrium that still maintains stability, and identify season duration and beetle reproduction rate as one of the major drivers of the steady state. These results also confirm the importance of Van Meerbeek's definition of stability, that multiple stability metrics are needed to assess regime-shift risk. Based on these results, we provide Table 1 that is likely to guide early warning signal detection based on the phenology variability measurement in the field and its likely direction of future regime, followed by Figure 1 that shows how these parameter variability adapts resistance and resilience in the system.

Figure 6 helps identify the distinct dynamics of resistance (R1) and resilience (R2) sensu Van Meerbeek [22] across the six parameters identified as potential early warning signal detectors through their covariance. The main purpose of this result is to validate our previous resistance and resilience metric, which helps us validate the previous set of results in light of adaptive stability theory. Also, it provides a comparative aspect to the result. Within the coexistence regime, R1 remains consistently high across all parameters. In contrast, R2 exhibits considerable variation within the same regime, indicating that the coexistence equilibrium can adapt to different resilience with the variability of these phenologies, while resistance can only change upon regime shift. Variability in susceptible beetle mortality is the only case where resilience R1 collapses. This is again another obvious assumption, as resistance is only observed when a perturbation is present; however, it still shows the differential behavior between stability components in this system. Observation of this obvious trend also helps validate our result from our model.

## 3.3 Meeting objective 3

Figure 7 shows how the timing and type of management affect cost savings in this eco-epidemic system to meet objective 3. Panels A and B show changes in control actions within each year. Panel C compares average effort per year per strategy. Within each season,

TABLE 1 Candidate early-warning signal matrix for regime shift (Objective 2).

| Parameter | Potential early warning signals | Likely alternative equilibrium |
|---|---|---|
| T (Season length) | Longer season → lower $R_P$ | Parasitoid-free |
| $\sigma_A$ (Beetle overwinter) | Higher survival → higher beetle density | Parasitoid-free |
| $\sigma_F$ (Parasitoid overwinter) | Higher survival → higher parasitoid | Coexistence maintained |
| $\mu_S$ (Larval mortality) | Lower $\mu_S$ → more larvae survive | Parasitoid-free |
| β (Parasitoid attack rate) | Higher β → stronger parasitoidism | Coexistence maintained |
| $R_B$ (Beetle reproduction) | Higher $R_B$ → stronger outbreaks | Parasitoid-free |

Each phenological scenario is characterized by its regime-shift probability (one-at-a-time variation), PRCC with the dominant eigenvalue magnitude $\rho^*$, the destabilizing direction of the corresponding parameter, the likely alternative equilibrium, and whether the phenological change is empirically observable. Parameters with regime-shift probability > 20% or |PRCC| > 0.25 that are empirically observable are classified as early-warning candidates.

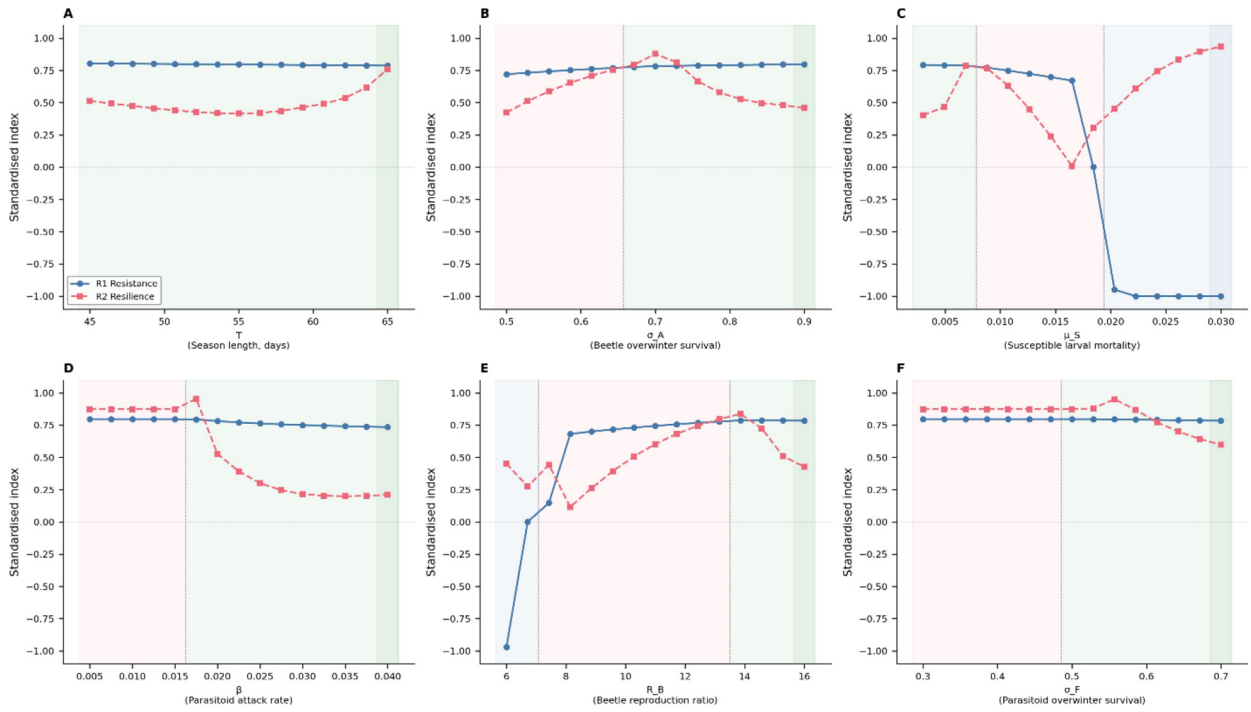


FIGURE 6
Resistance (R1) and resilience (R2) across the six candidate early-warning parameters identified in Figures 4, 5 and Table 1. **(A)** Season duration T. **(B)** Beetle overwinter survival $\sigma_A$. **(C)** Susceptible larval mortality $\mu_S$. **(D)** Parasitoid attack rate β. **(E)** Beetle reproduction ratio $R_B$. **(F)** Parasitoid overwinter survival $\sigma_F$. Background shading indicates the equilibrium regime (green: coexistence; pink: parasitoid-free; blue: canopy-only); dashed vertical lines mark transcritical bifurcation boundaries from Figure 3.

the three strategies differ in intervention focus and sequence. Strategy A relies solely on early parasitoid augmentation, i.e., the intentional release of parasitoid ($u_P$, Figure 7A) to maximize impact. Strategy B also begins with early parasitoid release, but later adds bird habitat enhancement, which reduces the need for additional augmentation. In contrast, Strategy C employs intensive early-season larval removal (Figure 7B), outperforming both parasitoid release and habitat improvements. Over multiple years (Figure 7C), effort allocation and cost trends diverge by strategy. All strategies have a peak within-season control in year 1, declining and stabilizing as the managed equilibrium is approached. In Strategy B, bird habitat enhancement ($u_B$) is key: early, cost-effective suppression is enabled by initial investment, which transitions to low maintenance and reduces future costs. Strategy C instead uses moderate $u_B$ in year, but emphasizes larval removal and parasitoid augmentation for short-term control, resulting in lower long-term maintenance costs once stabilized. Strategy A, in contrast, remains reliant on parasitoid release without bird habitat investment or intensive larval removal, leading to different cost dynamics over time. Each strategy's approach to initial investment, maintenance, and intervention mix yields unique cost-saving patterns. This highlights how explicit choices in management strategy shape both short- and long-term cost efficiency.

Figure 8 presents multi-year ecological outcomes for each management strategy, beginning from an outbreak state. Panel A shows seasonal cumulative defoliation (), while Panel B shows carrying capacity (). All strategies reduce defoliation below the threshold $D_{crit}$ in the first year, but Strategy C converges fastest, Strategy B is intermediate, and Strategy A stabilizes most slowly, with the most severe damage. Carrying capacity recovery

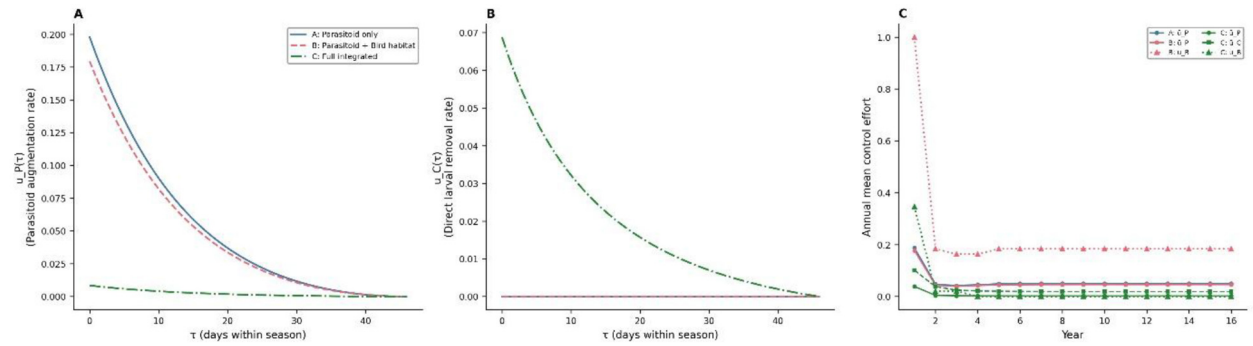


FIGURE 7
Optimal control allocation under three management scenarios. **(A)** Terminal within-season parasitoid augmentation rate. **(B)** Terminal within-season direct larval removal rate; active only in Scenario C. **(C)** Annual mean control effort over the 8-year planning horizon: mean within-season parasitoid augmentation (circles, solid), mean within-season direct removal (squares, dashed), and annual bird habitat enhancement (triangles, dotted).

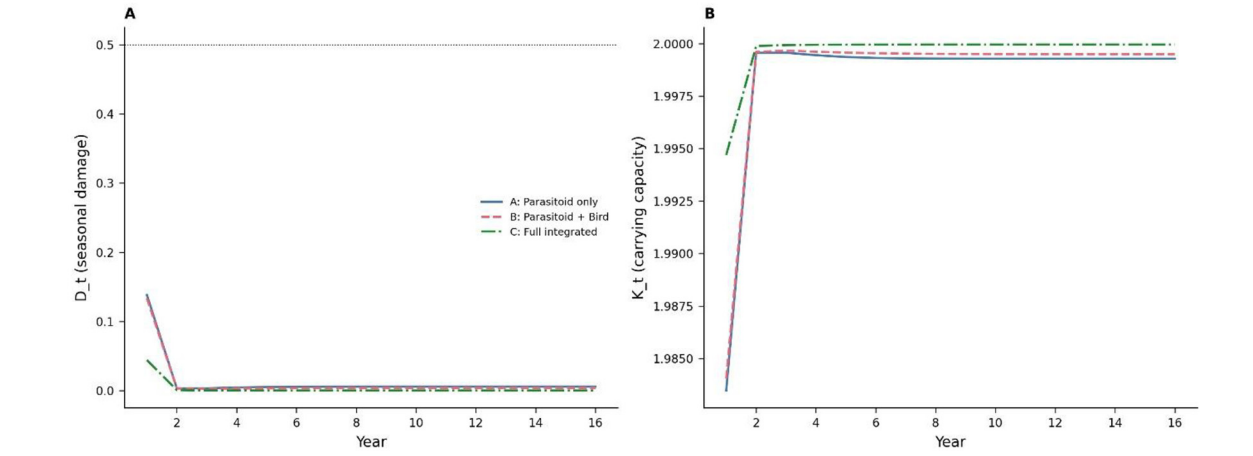


FIGURE 8
Multi-year state trajectories under three management scenarios. **(A)** Seasonal cumulative defoliation $D_t$ and **(B)** carrying capacity $K_t$ over the planning horizon. Dashed horizontal line in **(A)** marks the damage threshold.

follows the same ranking. Suppressing damage early reduces total defoliation, lessens the foliage-memory penalty (Equation 8), and lowers future intervention needs. For O3, the cost ranking from Figure 7 matches the ecological trajectory: the lowest-cost strategy achieves the fastest suppression and canopy recovery. According to the lexicographic decision rule outlined in the methodology, only Strategy C achieves local asymptotic stability at the managed equilibrium ($\rho^* = 0.98 < 1$). Strategies A ($\rho^* = 1.19$) and B ($\rho^* = 1.10$) exceed the stability boundary, rendering them infeasible despite reducing damage below. Strategy C is therefore the only feasible approach and also yields the minimum-cost outcome ($J = 14.0$, compared to 48.2 for A and 44.7 for B).

# 4 Discussion

Climate-driven phenological variability alters persistence and control within multitrophic systems [16, 44, 45]. Primary consumers typically advance their phenology faster than their natural enemies, creating trophic desynchrony that intensifies when multiple species shift simultaneously [44, 46]. This study models the Black alder–leaf beetle–parasitoid–generalist bird ecoepidemic system using a process-based, theory-driven framework. It couples within-season tri-trophic dynamics to interannual canopy feedback, following established hybrid host–parasitoid modeling practices [34, 42, 43]. The objectives were 3-fold: (i) identify the most probable stable equilibria across all phenological scenarios; (ii) quantify the likelihood of the system shifting from its current coexistence equilibrium to an undesirable state; and (iii) determine the minimal effort required for three pest-control strategies targeting the leaf beetle to prevent regime shifts across parameter space. The analysis used well-documented phenologies of the focal species [2, 7, 12] and applied optimal control theory to evaluate intervention effort [17]. Results show that the system does not consistently favor the most desirable coexistence equilibrium, aligning with classical host–parasitoid theory, which posits that stable coexistence occupies only a narrow parameter window [47–49]. Across the nine phenological scenarios, desirable coexistence (characterized by parasitoid persistence, low defoliation, and a maintained canopy) occurred only within a limited region of parameter space. The probability of regime shifts increased substantially when phenological parameters varied simultaneously, consistent with empirical evidence that asynchronous shifts across

trophic levels produce non-additive demographic consequences [44–46, 50, 51]. Only the fully integrated management strategy proved feasible across both seasonal and interannual scales. Model calibration was conducted within parameter ranges derived from literature on these phenologies across habitats containing the focal system (Annex 1 and 3). Consequently, the results do not constitute stand-level forecasts for any specific alluvial forest but provide a general understanding of the system's stability properties, including resilience and resistance dynamics, from an eco-epidemic perspective [22, 23, 39]. These stability properties may be observed in part or in full across European habitats containing the focal system.

The primary ecological implication of Objective 1 is that designating parasitoids as the main natural control for phyllophagous leaf beetle populations may undermine coexistence stability under phenological variability. Across the parameter space defined by phenological variability, stable equilibria occur more often in parasitoid-free and canopy-only states than in coexistence. Coexistence is maintained only when the parasitoid attack rate on beetles is high, both host and parasitoid populations have adequate overwintering survival, and generalist birds impose moderate predation pressure. These findings align with established host–parasitoid models, which show that coexistence within Nicholson–Bailey frameworks is limited to a narrow parameter range [49]. This outcome also supports evidence that phenological mismatch can destabilize tritrophic systems, even when pairwise interactions remain stable [51]. The increased prevalence of parasitoid-free and canopy-only stable equilibria under phenological variability offers insight into the difference between the desirability of coexistence in complex systems and the likelihood of convergence to a simpler, stable community structure. In this system, parasitoids help reduce the risk of future beetle outbreaks, while generalist birds use alternative, more abundant prey. These results are consistent with management strategies that prioritize augmenting natural enemies, although the success of such interventions depends on system-specific ecological conditions and requires empirical validation. The ecological theory of intraguild predation offers a comprehensive framework for validating management decisions, especially when direct empirical evidence is unavailable. Analogies with current findings can inform this validation. According to the theory, a higher-order predator suppresses an intermediate natural enemy while still reducing the shared prey [20, 52]. In the focal system, the direction and magnitude of bird predation on parasitised beetle larvae have not yet been quantified. Parasitised beetle larvae continue to feed until death is induced by the parasitoid [7] and remain vulnerable to bird predation during this time. Within the model, bird predation decreases the total larval pool and reduces defoliation. However, it also removes parasitised larvae before the koinobiont parasitoid completes development and emerges, causing lost recruitment opportunities for the endoparasitoid. Targeting parasite release at beetle foraging aggregations may increase the parasitoid's attack rate, as this cue is used to locate host beetle larvae [7]. The model indicates that increasing both the abundance and functional effectiveness of natural enemies could enhance system stability, pending empirical validation. In this context, coexistence loss is better characterized as a failure of parasitoid attack rather than a simple deficiency in parasite numbers.

Objective 2 extends Objective 1 by examining how phenological variation changes the probability of leaving coexistence. It quantifies the probabilities of each phenological variation that can cause a regime shift across any stable equilibrium. While Objective1/s prediction is limited to the initial state where the parasitoid is present, Objective 2 covers cases where the parasitoid is initially absent. A key difference is that a single parameter can affect two equilibria through different mechanisms. For example, season length does not visibly affect coexistence equilibria within the studied range except by drastically increasing defoliation damage. However, from a parasitoid-free initial state, season length can destabilize coexistence [49, 53]. Increased defoliation reduces the following year's carrying capacity through a memory effect driven by the accumulation of phytochemical defense [2, 13, 54]. The same defoliation also modifies canopy condition as a direct feedback [26]. Bird predation reduces defoliation damage once predator pressure exceeds a critical level [9, 55]. From the coexistence equilibrium, its net effect is moderated by opposing intraguild predation pathways because generalist birds simultaneously suppress the beetle and remove the parasitoid developing inside parasitised larvae [20, 52, 56, 57]. From a parasitoid-free equilibrium, bird predation does not directly alter parasitoid invasion risk because invasion success at that boundary depends on resident host density rather than the identity of the process suppressing it [58]. Phytochemical defense provides within-season resistance and accumulates as plant immunological memory [59, 60], feeding back into the following year's carrying capacity for both the beetle and its parasitoid [54, 61]. Nevertheless, this feedback has little influence on invasion thresholds or equilibrium class in our analysis. This observation warrants further study because the inter-annual accumulation rate and its quantitative effect on canopy regrowth remain poorly resolved under field conditions [13, 54, 61]. These results indicate that system dynamics operate on two distinct time scales. They establish that resistance and resilience at each time scale shape stability differently in this system. Within-season trophic interactions determine parasitoid invasion risk. Interannual canopy feedback driven by accumulated defoliation determines the quality and persistence of long-term equilibrium. This supports a multi-metric stability framework [22, 23]. Invasion, resistance, and resilience capture different but complementary aspects of regime-shift risk. Treating resistance and resilience as distinct stability metrics within the adaptive stability framework improves the interpretation of system behavior. High resistance across much of the coexistence regime implies that outbreak damage can remain low. However, resilience varies more strongly because recovery capacity can erode under phenological change. The system can look stable in the short term yet become dynamically fragile in the long term, as our findings show. Together, all the results of Objective 2 show that stability failure can occur through multiple distinct routes. Management should not infer security from low damage alone but evaluate invasion potential, recovery rate, and attractor-switch risk simultaneously.

In this study, we used eigenvalue-based and trajectory-based metrics to represent mechanistically distinct aspects of stability [23, 36, 39]. Within the Latin Hypercube sample, their correlation is positive but not perfect, consistent with prior evidence that resilience, resistance, and variability metrics are not mutually substitutable across ecosystems [23, 62]. Certain parameter sets

demonstrate that the eigenvalue indicates rapid return, while trajectory-based resilience remains low due to finite perturbations nearing the basin boundary, and the reverse can also occur [38, 63]. This decoupling is expected, because local eigenvalue analysis holds with certainty only for infinitesimal perturbations and carries no information about the distance to a basin boundary [36]. From an ecological perspective, eigenvalue-based resilience characterizes recovery from routine interannual fluctuations, whereas trajectory-based resilience characterizes recovery from discrete, large-amplitude disturbances — mapping, respectively, onto engineering and ecological resilience in the sense of Holling [39] [see also [36, 63]]. This distinction similarly separates the equilibrium damage margin from the transient resistance index. Reporting both metrics is therefore essential for distinguishing chronic degradation risk from acute perturbation risk, which is directly relevant for selecting between sustained and emergency management strategies [23, 64]. In addition to the probability of regime shift under this adaptive-stability framework, Objective 2 aims to identify potential early warning signals using three joint criteria. First, the parameter must contribute substantially to regime-shift probability. Second, it must show a partial rank correlation with the dominant eigenvalue indicating a destabilizing influence, following the standard LHS–PRCC sensitivity framework [65–67]. Third, the associated phenological process must be empirically observable during a simulation experiment searching for system destabilization. The candidate phenologies and their association with other phenologies, identified under Objective 2, are therefore proposed as ranked monitoring priorities rather than validated early warning signals capable of reliably indicating impending regime shifts, because our parameters come from multiple habitats and broader validation remains an open challenge in multi-trophic systems [63, 64, 68].

The three conditions we set for early warning signal identification are not interchangeable during system analyses [63, 68]. For example, a parameter may drive the dominant eigenvalue $\rho^*$ toward the stability boundary without greatly increasing regime-shift probability. Alternatively, a parameter may contribute to regime shifts but not be observable in practice. Among the identified candidates, season length is the most tractable: it can be measured with growing degree days, a validated tool for predicting insect phenology in integrated pest management [69] or with satellite-derived season-length products now available operationally at 10 m resolution across Europe [70]. By contrast, directly estimating the parasitoid attack rate or adult overwintering density requires intensive field sampling [11]; this has not yet been demonstrated at management-relevant scales in many systems [71]. These variables therefore provide a foundation for targeted monitoring designs and future studies on early warning signals in this system through phenologies. Collectively, these stability metrics capture distinct dimensions and should not be interpreted as interchangeable indicators of system robustness [23, 36, 62].

The management implication of this study follows from the optimal-control result in Objective 3. The result indicates that it is not simply that one strategy reduced beetle damage faster than the others. Under the study's lexicographic decision rule, a strategy is compared on cost only after it first proves ecologically feasible [17, 90]. In practical terms, the strategy must keep seasonal canopy loss below the critical damage level [26] and prevent the alder stand from slipping into a persistently degraded low-canopy condition [3, 41]. It must also maintain a long-term managed state in which parasitoids remain present and control continues after small disturbances [7, 20]. All three strategies reduced canopy damage below the critical level within the first year. However, only the fully integrated strategy (combining targeted larval removal, parasitoid release, and bird-habitat enhancement) met these broader conditions, consistent with the principles of integrated pest management, which combine multiple complementary tactics rather than rely on a single agent [72]. The parasitoid-only strategy and the parasitoid-plus-bird strategy both improved short-term suppression but did not produce a self-maintaining low-damage state in the long run, a pattern matching meta-analytical evidence that single-agent biological control rarely achieves durable pest regulation [73]. This distinction separates temporary outbreak suppression from durable restoration. The key result is that, under the model assumptions and feasibility constraints, the integrated strategy achieves both ecological stability and the lowest cost, although real-world implementation may be constrained by logistical, economic, and ecological factors not explicitly represented in the model. The superior performance of the integrated strategy is partly a structural consequence of the optimisation framework, because systems with more control variables generally achieve lower cost than subsets of controls [17, 74]. Beyond this structural effect, the ecological interpretation is that combined interventions enable simultaneous regulation of host density, support of natural enemies, and stabilization across temporal scales [52, 75]. Cost ranking therefore becomes meaningful only after the feasibility filter is passed. The ecological meanings used here follow the annex definitions of cumulative canopy damage, canopy availability, targeted larval removal, parasitoid release, and bird-habitat enhancement.

Our results from Objective 3 also suggest that intervention timing shapes the total effort required. Early action prevents current-season beetle damage from being carried over into the next year as a structural canopy penalty [2, 26]. In this ecoepidemic system, reducing larval density early in the outbreak lowers the total defoliation accumulated over the season and thereby weakens the foliage-memory feedback [13, 54, 61]. Without such suppression, heavy canopy loss reduces the forest's effective canopy support in the following year [3, 26], and the stand enters the next season in better condition when early control is applied. All three management strategies therefore concentrate most of their effort at the beginning of the intervention period and decline thereafter as the system approaches a lower-damage managed state—an allocation pattern consistent with general results from Pontryagin-type optimal control in biological systems, where the costate dynamics favor front-loaded effort when running state costs compound over time [17, 74]. Ecologically, this means the system responds best when control is applied before repeated feeding damage has accumulated enough to degrade future canopy recovery, consistent with broader evidence that early suppression minimizes long-run cost and outbreak-management failure in forest insect systems [76]. The exact schedule may differ under alternative recovery assumptions, climate forcing, or cost structures, but the general advantage of early, front-loaded action appears robust in this framework.Our study integrates processes often studied separately, such as seasonal beetle feeding, delayed parasitoid development, bird predation on both healthy and parasitised larvae, interannual canopy damage, and diverse

pest management. Structural robustness analyses confirm that all three qualitative conclusions are preserved when Beverton–Holt recruitment is replaced by the Ricker form (Annex 2, Table 2). Under Ricker recruitment, period-2 oscillations appear near bifurcation boundaries [34, 77], but these do not alter the dominant equilibrium class or strategy ranking.

The main contribution is a comprehensive systems-ecology framework that fills a literature gap on the structure-dependent multiple metrics defining adaptive stability properties in this system [22, 23]. From a modeling perspective, our study contributes by integrating an eco-epidemiological system that spans multiple trophic levels and exhibits intraguild predation [20, 52], and by embedding optimal control theory through habitat-management strategies as intervention measures [17]. By bridging the gap between host–parasitoid models that exclude plant feedback and higher-order predators [47, 48, 78] and plant-defense models that rarely assess management strategies [79], this study connects seasonal and annual phenology within a single hybrid framework [34, 77]. This unification enables analysis of immediate damage control, long-term recovery, regime shifts, and the most effective management options under optimal control theory. Varied parameter sources limit the results to a general outline, restricting direct implementation for a specific habitat without empirical data [11, 71]. With long-term field data on beetle outbreaks, parasitoid abundance, bird predation, and other life-cycle stages from a single habitat, the model could pinpoint regime-shift probability and equilibrium states more precisely. Such data would also test the early-warning signals identified here. Habitat-specific parameter values would narrow stability ranges and reveal how habitats distribute across the stability plane, informing prioritization of sites at risk of regime shift. The results should be interpreted as structural insights derived from a simplified model, rather than as direct predictions for specific forest systems.

To support this translational step, we provide AlderIPM-Sim Web (§2.6), which operationalises the multidimensional stability framework of Van Meerbeek et al. [22] as a reproducible exploration environment, an approach increasingly advocated for narrowing the gap between model development and ecological uptake [93]. Uncertainty in parameter values, variability across habitats, and unmodelled processes, such as explicit spatial structure [80], hyperparasitoidism [81], and species-specific trait-mediated behavioral responses [82], may influence real-world dynamics.

## Data availability statement

The original contributions presented in the study are included in the article/supplementary material, further inquiries can be directed to the corresponding author.

## Author contributions

SG: Investigation, Software, Visualization, Methodology, Conceptualization, Writing – original draft, Resources, Funding acquisition, Writing – review & editing, Validation, Project administration, Supervision, Formal analysis. SS: Writing – review & editing, Writing – original draft, Conceptualization.

## Funding

The author(s) declared that financial support was not received for this work and/or its publication.

## Acknowledgments

The authors used Opus 4.6 and Grammarly Pro as a language editing tool during manuscript preparation, including assistance with rephrasing and plagiarism checking. The analytical solutions and calculations were derived by MathLM Version: 11.3, IIASA (Mathematica B 0 2; MathKernel B 0 2; Sub Mathematica B 0 16; Sub MathKernel B 0 16).

## Conflict of interest

The author(s) declared that this work was conducted in the absence of any commercial or financial relationships that could be construed as a potential conflict of interest.

## Generative AI statement

The author(s) declare that Generative AI was used in the creation of this manuscript. The authors used Opus 4.6 and Grammarly Pro as a language editing tool during manuscript preparation, including assistance with rephrasing and plagiarism checking. The analytical solutions and calculations were derived by MathLM Version: 11.3, IIASA (Mathematica B 0 2; MathKernel B 0 2; Sub Mathematica B 0 16; Sub MathKernel B 0 16).

Any alternative text (alt text) provided alongside figures in this article has been generated by Frontiers with the support of artificial intelligence and reasonable efforts have been made to ensure accuracy, including review by the authors wherever possible. If you identify any issues, please contact us.

## Publisher's note



## Supplementary material

The Supplementary Material for this article can be found online at: https://www.frontiersin.org/articles/10.3389/fams.2026.1831903/full#supplementary-material

# References


1. European Commission. Council directive 92/43/EEC of 21 May 1992 on the conservation of natural habitats and of wild fauna and flora. *OJEC.* (1992) 206:7–50.

2. Dolch RT. Defoliation of alders (*Alnus glutinosa*) affects herbivory by leaf beetles on undamaged neighbours. *Oecologia.* (2000) 125:504–11. doi: 10.1007/s004420000482

3. Valor T, Camprodon J, Buscarini S, Casals P. Drought-induced dieback of riparian black alder as revealed by tree rings and oxygen isotopes. *Forest Ecol Manage.* (2020) 478:118500. doi: 10.1016/j.foreco.2020.118500

4. Hart AT, Landhäusser SME. Tracing carbon and nitrogen reserve remobilization during spring leaf flush and growth following defoliation. *Tree Physiol.* (2024) 44:tpae015. doi: 10.1093/treephys/tpae015

5. Barker Plotkin A, Blumstein M, Laflower D, Pasquarella VJ, Chandler JL, Elkinton JS, et al. Defoliated trees die below a critical threshold of stored carbon. *Funct Ecol.* (2021) 35:2156–67. doi: 10.1111/1365-2435.13891

6. Miranda JC, Rodríguez-Calcerrada J, Pita P, Saurer M, Oleksyn J, Gil L, et al. Carbohydrate dynamics in a resprouting species after severe aboveground perturbations. *Eur J For Res.* (2020) 139:841–52. doi: 10.1007/s10342-020-01288-2

7. Stireman JOIII, O'Hara JE, Wood DM. Tachinidae: evolution, behavior, and ecology. *Annu Rev Entomol.* (2006) 51:525–55. doi: 10.1146/annurev.ento.51.110104.151133

8. Remmel T, Davison J, Tammaru T. Quantifying predation on folivorous insect larvae: the perspective of life-history evolution. *Biol J Linn Soc.* (2011) 104:1–18. doi: 10.1111/j.1095-8312.2011.01721.x

9. Monteagudo N, Benayas JMR, Andivia E, Rebollo S. Avian regulation of crop and forest pests: a meta-analysis. *Pest Manag Sci.* (2023) 79:4690–9. doi: 10.1002/ps.7421

10. Kepenekci II. A new biopesticide from a local *Bacillus thuringiensis* var. *tenebrionis* (Xd3) against alder leaf beetle (Coleoptera: Chrysomelidae). *World J Microbiol Biotechnol.* (2017) 33:95. doi: 10.1007/s11274-017-2263-0

11. van Driesche RG, Hoddle MS, Center TD. *Control of Pests and Weeds by Natural Enemies: An Introduction to Biological Control.* Hoboken, NJ: Blackwell Publishing (2008).

12. Sivrikaya R, Altun N, Faiz Ö. Diet-mediated modulation on the development and phenoloxidase activity in the alder leaf beetle larvae, *Agelastica alni* (L., 1758) (Coleoptera: Chrysomelidae). *Turk J Entomol.* (2020) 44:193–202. doi: 10.16970/entoted.600893

13. Tscharntke T, Thiessen S, Dolch R, Boland W. Herbivory, induced resistance, and interplant signal transfer in *Alnus glutinosa*. *Biochem Syst Ecol.* (2001) 29:1025–47. doi: 10.1016/S0305-1978(01)00048-5

14. Pasteels JM, Daloze D, Rowell-Rahier M. Chemical defence in chrysomelina leaf beetles: Secreting and volatile compounds. *Arch Insect Biochem Physiol.* (1995) 29:85–94.

15. Stephens DW, Krebs JR. *Foraging Theory*. Princeton, NJ: Princeton University Press (1986).

16. Renner SS, Zohner CM. Climate change and phenological mismatch in trophic interactions among plants, insects, and vertebrates. *Annu Rev Ecol Evol Syst.* (2018) 49:165–82. doi: 10.1146/annurev-ecolsys-110617-062535

17. Lenhart SJT. *Optimal Control Applied to Biological Models.* New York, NY: Chapman and Hall/CRC (2007).

18. Segoli M, Papegay Y, Rozenberg T, Wajnberg E. Why do predators attack parasitized prey? Insights from a probabilistic model and a literature survey. *Behav Process.* (2024) 216:105002. doi: 10.1016/j.beproc.2024.105002

19. Polis GA, Myers CA, Holt RD. The ecology and evolution of intraguild predation. *Annu Rev Ecol Syst.* (1989) 20:297–330. doi: 10.1146/annurev.es.20.110189.001501

20. Rosenheim JA. Higher-order predators and the regulation of insect herbivore populations. *Annu Rev Entomol.* (1998) 43:421–47. doi: 10.1146/annurev.ento.43.1.421

21. Fakhry NH, Naji RK, Smith SR, Haque M. Prey fear of a specialist predator in a tri-trophic food web can eliminate the superpredator. *Front Appl Mathemat Statist.* (2022) 8:963991. doi: 10.3389/fams.2022.963991

22. Van Meerbeek K, Jucker T, Svenning J-C. Unifying the concepts of stability and resilience in ecology. *J Ecol.* (2021) 109:3114–32. doi: 10.1111/1365-2745.13651

23. Donohue I, Hillebrand H, Montoya JM, Petchey OL, Pimm SL, Fowler MS, et al. Navigating the complexity of ecological stability. *Ecol Lett.* (2016) 19:1172–85. doi: 10.1111/ele.12648

24. Hillebrand H, Blasius B, Borer ET, Chase JM, Downing JA, Eriksson BK, et al. Biodiversity change is uncoupled from species richness trends: consequences for conservation and monitoring. *J Appl Ecol.* (2018) 55:169–84. doi: 10.1111/1365-2664.12959

25. Hawkins BA. Pattern and process in host–parasitoid interactions. *Ecol Monogr.* (1994) 64:297–323. doi: 10.1017/CBO9780511721885

26. Ferretti M, Bacaro G, Brunialti G, Calderisi M, Croisé L, Frati L, et al. Tree canopy defoliation can reveal growth decline in mid-latitude temperate forests. *Ecol Indic.* (2021) 127:107749. doi: 10.1016/j.ecolind.2021.107749

27. Beverton RJHSJ. *On the Dynamics of Exploited Fish Populations*. London: HMSO (1957).

28. Grégoire J-C. *Larval Gregariousness in the Chrysomelidae*. In: Jolivet P, Petitpierre E, Hsiao TH, editors. *Biology of Chrysomelidae*. Dordercht: Kluwer Academic Publishers (1988). p. 253–60.

29. McAvoy TJ, Kok LT, Mays WT. Neonate *Galerucella calmariensis* (Coleoptera: Chrysomelidae) response to larval density and host plant quality. *Environ Entomol.* (2002) 31:880–6. doi: 10.1603/0046-225X-31.5.880

30. Herzig AL. Effects of population density on long-distance dispersal in the goldenrod beetle *Trirhabda virgata*. *Ecology.* (1995) 76:2044–54. doi: 10.2307/1941679

31. Chapman DS, Dytham CGS. Landscape and fine-scale movements of a leaf beetle: the importance of boundary behaviour. *Oecologia.* (2007) 154:55–64. doi: 10.1007/s00442-007-0806-z

32. van den Driessche P, Watmough J. Reproduction numbers and sub-threshold endemic equilibria for compartmental models of disease transmission. *Math Biosci.* (2002) 180:29–48. doi: 10.1016/S0025-5564(02)00108-6

33. Kuznetsov YA. *Elements of Applied Bifurcation Theory (3rd ed.)*. New York, NY: Springer (2004).

34. Kot M. *Elements of Mathematical Ecology*. Cambridge: Cambridge University Press (2001).

35. Pimm SL. The complexity and stability of ecosystems. *Nature.* (1984) 307:321–6. doi: 10.1038/307321a0

36. Arnoldi J-F, Loreau MB. Resilience, reactivity and variability: a mathematical comparison of ecological stability measures. *J Theoret Biol.* (2016) 389:101–12. doi: 10.1016/j.jtbi.2015.10.012

37. Medeiros LP, Song C, Saavedra S. Merging dynamical and structural indicators to measure resilience in multispecies systems. *J Anim Ecol.* (2021) 90:2384–97. doi: 10.1111/1365-2656.13421

38. Menck PJ, Heitzig J, Marwan N, Kurths J. How basin stability complements the linear-stability paradigm. *Nat Phys.* (2013) 9:89–92. doi: 10.1038/nphys2516

39. Holling CS. Resilience and stability of ecological systems. *Annu Rev Ecol Syst.* (1973) 4:1–23. doi: 10.1146/annurev.es.04.110173.000245

40. Folke C, Hahn T, Olsson PJ. Adaptive governance of social-ecological systems. *Annu Rev Environ Resour.* (2005) 30:441–73. doi: 10.1146/annurev.energy.30.050504.144511

41. Scheffer M, Carpenter S, Foley JA, Folke C, Walker B. Catastrophic shifts in ecosystems. *Nature.* (2001) 413:591–6. doi: 10.1038/35098000

42. Chattopadhyay JO. A predator–prey model with disease in the prey. *Nonlinear Analysis.* (1999) 36:747–66. doi: 10.1016/S0362-546X(98)00126-6

43. Hethcote HW, Wang W, Han LZ. A predator–prey model with infected prey. *Theor Popul Biol.* (2004) 66:259–68. doi: 10.1016/j.tpb.2004.06.010

44. Thackeray SJ, Henrys PA, Hemming D, Bell JR, Botham MS, Burthe S, et al. Phenological sensitivity to climate across taxa and trophic levels. *Nature.* (2016) 535:241–5. doi: 10.1038/nature18608

45. Both C, Van Asch M, Bijlsma RG, Van Den Burg ABME. Climate change and unequal phenological changes across four trophic levels: constraints or adaptations? *J Anim Ecol.* (2009) 78:73–83. doi: 10.1111/j.1365-2656.2008.01458.x

46. Visser ME, Both C. Shifts in phenology due to global climate change: the need for a yardstick. *Proc R Soc B Biol Sci.* (2005) 272:2561–9. doi: 10.1098/rspb.2005.3356

47. Nicholson AJ, Bailey VA. The balance of animal populations. Part I. *Proc Zool Soc London.* (1935) 105:551–98. doi: 10.1111/j.1096-3642.1935.tb01680.x

48. Hassell MP, Lawton JHRM. Patterns of dynamical behaviour in single-species populations. *J Anim Ecol.* (1976) 45:471–86. doi: 10.2307/3886

49. Singh A. Nicholson–Bailey models with aggregated parasitoidism: analysis and implications. *PLoS ONE.* (2023) 18:e0283874. doi: 10.1371/journal.pone.0283874

50. Tougeron K, Brodeur J, Le Lann C, van Baaren J. How climate change affects the seasonal ecology of insect parasitoids. *Ecol Entomol.* (2019) 45:167–81. doi: 10.1111/een.12792

51. Belitz MW, Barve V, Guralnick RP, Zipkin EFJM. Potential for bird–insect phenological mismatch in a tri-trophic system. *J Anim Ecol.* (2025) 94:717–28. doi: 10.1111/1365-2656.70007

52. Polis GA, Holt RD. Intraguild predation: the dynamics of complex trophic interactions. *Trends Ecol Evolut.* (1992) 7:151–4. doi: 10.1016/0169-5347(92)90208-S

53. Emerick BKA. The effects of host-feeding on stability of discrete-time host–parasitoid population dynamic models. *Math Biosci.* (2016) 272:54–63. doi: 10.1016/j.mbs.2015.11.011

54. Schott J, Jantzen F, Hilker M. Elm tree defences against a specialist herbivore are inducible in neighbouring trees. *Tree Physiol.* (2023) 43:1216–32. doi: 10.1093/treephys/tpad038

55. Böhm SM, Wells KEKV. Top-down control of herbivory by birds and bats in the canopy of temperate broadleaved oaks (*Quercus robur*). *PLoS ONE.* (2011) 6:e17857. doi: 10.1371/journal.pone.0017857

56. Holt RDGA. A theoretical framework for intraguild predation. *Am Nat.* (1997) 149:745–64. doi: 10.1086/286018

57. Holt RDGR. Alternative prey and the dynamics of intraguild predation: theoretical perspectives. *Ecology.* (2007) 88:2706–12. doi: 10.1890/06-1525.1

58. Hochberg MERD. *Biogeographical Perspectives on Arms Races*. In: Dieckmann U, Metz JAJ, Sabelis MW, Sigmund K, editors. *Adaptive dynamics of infectious diseases: in pursuit of virulence management*. New York, NY: Cambridge University Press. (2002). p. 197–209.

59. Conrath U, Beckers GJM, Langenbach CJGMR. Priming for enhanced defense. *Annu Rev Phytopathol.* (2015) 53:97–119. doi: 10.1146/annurev-phyto-080614-120132

60. Song GC, Choi HK, Kim YS, Choi JS, Ryu C-M. Seed defense biopriming with bacterial cyclodipeptides triggers immunity in cucumber and pepper. *Sci Rep.* (2018) 8:11493. doi: 10.1038/s41598-017-14155-9

61. Karban R, Ishizaki S, Shiojiri K. Long-term demographic consequences of eavesdropping for sagebrush. *J Ecol.* (2012) 100:932–8. doi: 10.1111/j.1365-2745.2012.01974.x

62. Keersmaecker De W, Lhermitte S, Honnay O, Tenhunen J, Somers B, Coppin P. How to measure ecosystem stability? An evaluation of the reliability of stability metrics based on remote sensing time series across the major global ecosystems. *Glob Chang Biol.* (2014) 20:2149–61. doi: 10.1111/gcb.12495

63. Dakos V, Carpenter SR, van Nes EHM. Resilience indicators: prospects and limitations for early warnings of regime shifts. *Philos Trans R Soc London B Biol Sci.* (2015) 370:20130263. doi: 10.1098/rstb.2013.0263

64. Lindegren M, Dakos V, Gröger JP, Gårdmark A, Kornilovs G, Otto SA, et al. Early detection of ecosystem regime shifts: a multiple method evaluation for management application. *PLoS ONE.* (2012) 7:e38410. doi: 10.1371/journal.pone.0038410

65. Blower SMH. Sensitivity and uncertainty analysis of complex models of disease transmission: an HIV model, as an example. *Int Stat Rev.* (1994) 62:229–43. doi: 10.2307/1403510

66. Marino S, Hogue IB, Ray CJ, Kirschner DE. A methodology for performing global uncertainty and sensitivity analysis in systems biology. *J Theor Biol.* (2008) 254:178–96. doi: 10.1016/j.jtbi.2008.04.011

67. Saltelli A, Ratto M, Andres T, Campolongo F, Cariboni J, Gatelli D, et al. *Global Sensitivity Analysis: The Primer*. Chichester: Wiley (2008).

68. Scheffer M, Bascompte J, Brock WA, Brovkin V, Carpenter SR, Dakos V, et al. Early-warning signals for critical transitions. *Nature.* (2009) 461:53–9. doi: 10.1038/nature08227

69. Herms DA. *Using Degree-Days and Plant Phenology to Predict Pest Activity*. In: Krischik V, Davidson J, editors. *IPM (Integrated Pest Management) of Midwest Landscapes*. University of Minnesota: Minnesota Agricultural Experiment Station Publication SB-07645 (2004). p. 49–59.

70. Copernicus Land Monitoring Service. *High Resolution Vegetation Phenology and Productivity (HR-VPP)* (2021). Available online at: https://land.copernicus.eu/en/products/vegetation (Accessed April 23, 2026).

71. Gould JR, Elkinton JS, Van Driesche RG. Assessment of potential methods of measuring parasitism by Brachymeria intermedia (Nees) (Hymenoptera: Chalcididae) of Pupae of the Gypsy Moth. *Environ Entomol.* (1992) 21:394–400. doi: 10.1093/ee/21.2.394

72. Barzman M, Bàrberi P, Birch ANE, Boonekamp P, Dachbrodt-Saaydeh S, Graf B, et al. Eight principles of integrated pest management. *Agron Sustain Dev.* (2015) 35:1199–215. doi: 10.1007/s13593-015-0327-9

73. Stiling P, Cornelissen T. What makes a successful biocontrol agent? A meta-analysis of biological control agent performance. *Biol Control.* (2005) 34:236–46. doi: 10.1016/j.biocontrol.2005.02.017

74. Pontryagin LS, Boltyanskii VG, Gamkrelidze RV, Mishchenko EF. *The Mathematical Theory of Optimal Processes*. New York, NY: Wiley (1962).

75. Letourneau DK, Jedlicka JA, Bothwell SG, Moreno CR. Effects of natural enemy biodiversity on the suppression of arthropod herbivores in terrestrial ecosystems. *Annu Rev Ecol Evol Syst.* (2009) 40:573–92. doi: 10.1146/annurev.ecolsys.110308.120320

76. Liebhold AM, Tobin PC. Population ecology of insect invasions and their management. *Annu Rev Entomol.* (2008) 53:387–408. doi: 10.1146/annurev.ento.52.110405.091401

77. Elaydi SN. *An Introduction to Difference Equations (3rd ed.)*. New York, NY: Springer (2005)

78. Ji H, Vasilyeva M, Mbroh NAA. Epidemic dynamics in the spatiotemporal predator–prey model. *Front Appl Mathemat Statist.* (2025) 11:1642676. doi: 10.3389/fams.2025.1642676

79. Hakes ASJT. Successional change in plant resistance and tolerance to herbivory. *Ecology.* (2012) 93:1059–70. doi: 10.1890/10-1637.1

80. Hassell MP. *The Spatial and Temporal Dynamics of Host–Parasitoid Interactions*. Oxford: Oxford University Press (2000).

81. Sullivan DJ, Völkl W. Hyperparasitism: multitrophic ecology and behavior. *Annu Rev Entomol.* (1999) 44:291–315. doi: 10.1146/annurev.ento.44.1.291

82. Schmitz OJ. Effects of predator hunting mode on grassland ecosystem function. *Science.* (2008) 319:952–4. doi: 10.1126/science.1152355

83. Cornell HVBA. Survival patterns and mortality sources of herbivorous insects: some demographic trends. *Am Nat.* (1995) 145:563–93. doi: 10.1086/285756

84. Wiggins S. *Introduction to Applied Nonlinear Dynamical Systems and Chaos (2nd ed.)*. New York, NY: Springer (2003).

85. Mols CMM, Visser ME. Great tits can reduce caterpillar damage in apple orchards. *J Appl Ecol.* (2002) 39:888–99. doi: 10.1046/j.1365-2664.2002.00761.x

86. Hartman P. *Ordinary Differential Equations*. New York, NY: Wiley (1964).

87. Allgower ELK. *Introduction to Numerical Continuation Methods*. Philadelphia, PA: SIAM (2003).

88. Gregory RD, Vorisek P, Noble DG, Van Strien A, Klvanova A, Eaton M, et al. The generation and use of bird population indicators in Europe. *Bird Conserv Int.* (2008) 18:244. doi: 10.1017/S0959270908000312

89. Fleming WH, Raymond W. *Deterministic and Stochastic Optimal Control*. Berlin: Springer (1975).

90. Blanchini F. Set invariance in control. *Automatica.* (1999) 35:1747–67. doi: 10.1016/S0005-1098(99)00113-2

91. Walker B, Holling CS, Carpenter SR, Kinzig A. Resilience, adaptability and transformability in social–ecological systems. *Ecol Soc.* (2004) 9:5. doi: 10.5751/ES-00650-090205

92. Khalil HK. *Nonlinear Systems (3rd ed.)*. Upper Saddle River, NJ: Prentice Hall (2002).

93. Jakeman AJ, Elsawah S, Wang H-H, Hamilton SH, Melsen L, Grimm V. Towards normalizing good practice across the whole modeling cycle: its instrumentation and future research topics. Socio Environ Syst Model. (2024) 6:18755. doi: 10.18174/sesmo.18755